The Journal of Experimental Biology 215, 4070-4084

doi:10.1242/jeb.075044

## RESEARCH ARTICLE

# Wingbeat kinematics and motor control of yaw turns in Anna's hummingbirds (*Calypte anna*)

Douglas L. Altshuler[1,2,*], Elsa M. Quicazán-Rubio[1,†], Paolo S. Segre[1,2] and Kevin M. Middleton[3]

[1]Department of Biology, University of California, Riverside, Riverside, CA 92521, USA, [2]Department of Zoology, University of British Columbia, Vancouver, Canada, BC, V6T 1Z4 and [3]Department of Pathology and Anatomical Sciences, University of Missouri, Columbia, MO 65212, USA

*Author for correspondence (doug@zoology.ubc.ca)

[†]Present address: Experimental Zoology Group, Wageningen University, 6700 AH Wageningen, The Netherlands

## SUMMARY

**The biomechanical and neuromuscular mechanisms used by different animals to generate turns in flight are highly variable. Body size and body plan exert some influence, e.g. birds typically roll their body to orient forces generated by the wings whereas insects are capable of turning *via* left–right wingbeat asymmetries. Turns are also relatively brief and have low repeatability, with almost every wingbeat serving a different function throughout the change in heading. Here we present an analysis of Anna's hummingbirds (*Calypte anna*) as they fed continuously from an artificial feeder revolving around the outside of the animal. This setup allowed for examination of sustained changes in yaw without requiring any corresponding changes in pitch, roll or body position. Hummingbirds sustained yaw turns by expanding the wing stroke amplitude of the outer wing during the downstroke and by altering the deviation of the wingtip path during both downstroke and upstroke. The latter led to a shift in the inner–outer stroke plane angle during the upstroke and shifts in the elevation of the stroke plane and in the deviation of the wingtip path during both strokes. These features are generally more similar to how insects, as opposed to birds, turn. However, time series analysis also revealed considerable stroke-to-stroke variation. Changes in the stroke amplitude and the wingtip velocity were highly cross-correlated, as were changes in the stroke deviation and the elevation of the stroke plane. As was the case for wingbeat kinematics, electromyogram recordings from pectoral and wing muscles were highly variable, but no correlations were found between these two features of motor control. The high variability of both kinematic and muscle activation features indicates a high level of wingbeat-to-wingbeat adjustments during sustained yaw. The activation timing of the muscles was more repeatable than the activation intensity, which suggests that the former may be constrained by harmonic motion and that the latter may play a large role in kinematic adjustments. Comparing the revolution frequency of the feeder with measurements of free flight yaws reveals that feeder tracking, even at one revolution every 2 s, is well below the maximum yaw capacity of the hummingbirds.**

Supplementary material available online at http://jeb.biologists.org/cgi/content/full/215/23/4070/DC1

Key words: biomechanics, electromyography, flight, hummingbird, maneuvering, neuromuscular control.

Received 15 May 2012; Accepted 9 August 2012

## INTRODUCTION

Flying animals have the ability to alter velocity and orientation about three axial and three torsional degrees of freedom with varying degrees of independence. This ability is generally termed maneuverability (Dudley, 2000), but this definition does not provide a specific metric that can be compared across individuals or among taxa. Studies with flying birds and bats have sometimes used a specific definition of maneuverability as the smallest radius for which a given animal can make a turn (Pennycuick, 1975). This value is invariant for hovering insects and hummingbirds, which can turn in place. The turning performance of many taxa across a broad range of body sizes has been examined, including insects (Fry et al., 2003; Ristroph et al., 2009; Springthorpe et al., 2012; Hedrick et al., 2009), fishes (Weihs, 1972; Webb, 1983), birds (Warrick et al., 1988; Warrick and Dial, 1998; Hedenström and Rosén, 2001; Hedrick and Biewener, 2007; Hedrick et al., 2007; Ros et al., 2011), bats (Norberg and Rayner, 1987; Iriarte-Díaz and Swartz, 2008), carnivorous mammals (Eilam, 1994) and humans (Carrier et al., 2001; Lee et al., 2001). These studies have revealed a diversity of biomechanical mechanisms for turning, even within clades of flying animals such as birds or insects. One source of this variation is that turns can be composed of different magnitudes and phases of body pitch, roll and yaw. Thus, even for a specific definition of maneuverability in flight, it is unknown which, if any, kinematic features are necessarily conserved among animal species or across body sizes.

Hovering insects and hummingbirds provide an opportunity for comparing maneuvering performance because these animals can all turn in place about the yaw axis with little or no change about roll and pitch axes and no change in horizontal or vertical position. Experiments with tethered fruit flies [*Drosophila melanogaster* (Götz, 1968)] and locusts [*Locusta migratoria* (Dawson et al., 1997)] have demonstrated that during attempted turns, the inner wing (the inner forewing for the locusts) sweeps through a smaller arc, i.e. has lower stroke amplitude, compared with the outer wings. Tethered locusts also exhibit a pronounced asymmetry in the average elevation of the forewings, with the inner wing being more depressed (Dawson et al., 1997). When generating yaw turns in free flight,

the outer wing of *D. melanogaster* has a wider stroke amplitude and a more horizontal stroke, i.e. a shallower stroke plane angle, which also causes an increase in the angle of attack of the outer wing (Fry et al., 2003). A universal mechanism for terminating yaw turns in freely flying insects and hummingbirds is the use of symmetrical wingbeat kinematics because the difference in velocity experienced by each wing during the turn is sufficient to damp the yaw torque (Hedrick et al., 2009). The kinematic mechanisms that hummingbirds use to generate yaw turns have not been investigated previously, although more complicated escape maneuvers have been described (Clark, 2011).

Any difference between left and right wingbeat kinematics must be reflected in the activation features of at least one bilateral pair of muscles. Numerous recordings from the basalar muscles of tethered insects have revealed that the activation phase and number of spikes are associated with changes in wing deviation and stroke amplitude (Dawson et al., 1997; Tu and Dickinson, 1996; Lehmann and Götz, 1996). When larger groups of muscles are recorded simultaneously, subsets have been found to act synergistically (Heide, 1975). For example, two of the basalar muscles of tethered blowflies (*Calliphora vicina*) are associated with wing downstroke deviation, and interactions among basalar and pterale III muscles influence the stroke amplitude (Balint and Dickinson, 2001). Recordings from freely flying convolvulus hawkmoths [*Agrius convolvuli* (Ando et al., 2002)] further demonstrate associations between the timing on direct muscles in the insect thorax and the stroke amplitude and deviation (Wang et al., 2008). Timing differences in the main power muscles, the dorsal longitudinal and dorsal ventral muscles, of the tobacco hawkmoth (*Manduca sexta*) influences the overall yaw velocity of the body in free flight, but do so by acting upon the inertial velocity that is extended from the previous stroke (Springthorpe et al., 2012).

The activation patterns of avian muscles are more difficult to interpret because the large number of motoneurons innervating each muscle leads to considerable variation in timing (temporal recruitment patterns) and intensity (spatial recruitment patterns). Hedrick and Biewener (Hedrick and Biewener, 2007) recorded from two pectoral muscles (pectoralis major and supracoracoideus) and two wing muscles (biceps brachii and extensor metacarpi radialis) as rose-breasted cockatoos (*Eolophus roseicapillus*) navigated a 90 deg turn. They observed left–right activation asymmetries in all of the muscles, but none of these patterns were associated with among-wingbeat changes in body kinematics. Hummingbirds can hover like many insects and, during this behavior, the pectoralis major has a relatively simple activation pattern composed of only one to three spikes (Hagiwara et al., 1968). Experiments in low-density air, during load lifting and in a wind tunnel demonstrate an association between the maximum electromyogram (EMG) spike amplitude from this muscle and the wingstroke amplitude (Altshuler et al., 2010; Tobalske et al., 2010). The hummingbird therefore presents an opportunity to examine neuromuscular and kinematic mechanisms of turning in birds that can be directly compared with the extensive literature on insect flight control.

For the present study, we sought to address three questions: (1) what are the wingbeat kinematic and neuromuscular features used by hummingbirds to generate sustained yaw turns; (2) how repeatable are these features; and (3) what are the temporal associations between muscle activation patterns and wingbeat kinematics? To address these questions, we trained hummingbirds to track a feeder that revolved around the outside of the animal, thereby eliciting a pure yaw turn, without any change in roll, pitch, horizontal or vertical position. The hummingbirds tracked the feeder for several seconds, amounting to as many as a hundred or more wingbeats. During these steady-state maneuvers, we recorded the wingbeat kinematics using high-speed cameras and made EMG recordings from the pectoralis major, pronator profundus and pronator superficialis muscles. Associations among kinematic and electrophysiological variables are examined using several statistical approaches including time series analysis.

## MATERIALS AND METHODS

### Animals

Between May and September 2009, we captured four adult male Anna's hummingbirds [*Calypte anna* (Lesson 1829)] at the University of California, Riverside campus, using portable drop-door traps and Hall traps (Russell and Russell, 2001). The hummingbirds were housed individually in cages measuring $0.93\times0.62\times0.62$ m and fed *ad libitum* with a solution of 13% artificial nectar (Nektar-Plus, Nekton, Pforzheim, Germany) and 5% sucrose. The light cycle in the vivarium was 12 h:12 h light:dark with lights on from 07:00 to 19:00 h. Prior to experiments, the animals were brought to the laboratory for 3–4 days of training and acclimation to the flight chamber. All the procedures were conducted under permits from the United States Fish and Wildlife Service and the California Department of Fish and Game, and approved by the Institutional Animal Care and Use Committee at the University of California, Riverside.

### Experimental setup and training

The flight chamber (Fig. 1A) was 0.61 m high, 0.58 m deep and 0.51 m wide and contained a wooden perch in one corner and an artificial feeder made out of a 1 ml syringe that was mounted at the end of a J-shaped aluminum arm. The long arm was connected to a stepper motor (MDrive 23 Plus, Schneider Electric Motion, Marlborough, CT, USA) placed in the center of the cage roof. The distance between the mouth of the feeder and the axis of rotation of the motor was adjusted slightly, if needed, for each bird such that they could feed from the revolving syringe while maintaining their center of gravity in the axis of feeder rotation, thereby executing a pure yaw turn.

An individual hummingbird was initially moved from the vivarium, placed in the experimental chamber, and trained for the experiment. They first learned to feed on command from the stationary feeder by covering it for 20 min in between feeding bouts. As soon as a bird terminated a feeding bout by flying away, the feeder was once again covered. Within 1 to 3 h, each bird learned to approach the feeder as soon as access was allowed and then feed for bouts longer than 5 s. Thereafter, the bird learned to feed while the feeder was rotated at a slow frequency of 7.5 r.p.m. We maintained this frequency until the hummingbird consistently followed the feeder for 2 s and then increased the revolution frequencies to 15, 25 and finally 30 r.p.m., which was the frequency used for all experiments with the turning feeder. The birds were trained equally on both clockwise and counterclockwise directions at all training frequencies. Each hummingbird typically required 3 days of training, 4 h per day before they could follow the feeder consistently at 30 r.p.m. (0.5 Hz).

### Surgery and experimental procedures

Hummingbirds were anesthetized with isoflurane during the surgical procedure to implant the EMG and ground wires. Induction concentrations were 2.5%, but the isoflurane concentration was brought to 1.8% as quickly as possible once the animals reached a surgical plane. Oxygen flow rates were maintained at 500 cc $min^{-1}$.

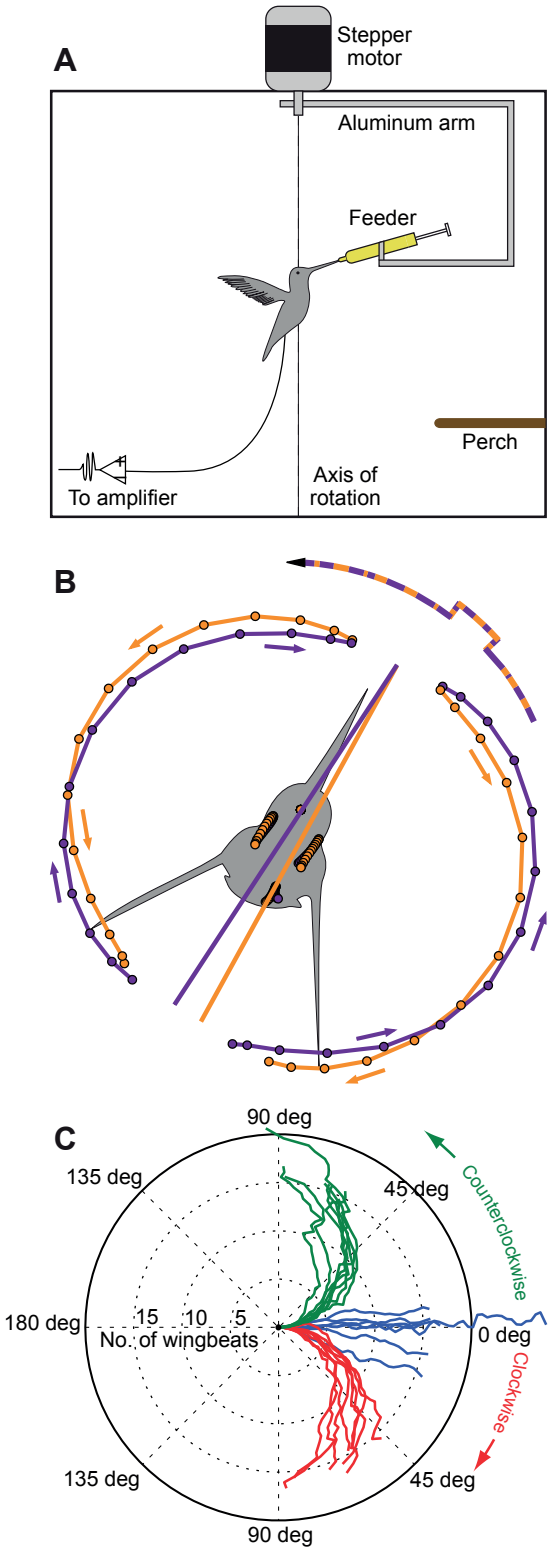


Fig. 1. Hummingbirds performed yaw turns while tracking a revolving feeder in a flight chamber (A). The feeder was mounted to a J-shaped aluminum arm that was itself connected to a stepper motor. The arm was adjusted for each bird so that the bird's center of mass was located at the motor's axis of rotation. The feeder was covered between feeding trials and the bird was provided with a perch at all times. Electromyograms from up to four muscles were recorded using trailing leads that connected to an extracellular amplifier. The frame of reference was defined in part by the position of the wings for each stroke (B). Downstrokes are indicated in orange with the tail, shoulder and wingtip positions indicated by a point for each video frame. Upstrokes are indicated in purple. The angular change in the wingbeat-centered frame of reference between strokes is given by the yaw angle Ψ. In this example from a counterclockwise turn, the Ψ values for 29 sequential strokes are depicted in the maroon–orange curve. The indent represents several strokes during which the hummingbird did not vary Ψ. The Ψ values for all of the hummingbirds included in the study are provided in a polar diagram (C). Any change along the radius indicates a change in Ψ for that stroke. The sequences differed with respect to the number of wingbeats digitized. Experiments are color coded with blue indicating hovering at the stationary feeder, and green and red indicating feeder revolution in the counterclockwise and clockwise directions, respectively.

Each animal had four recording electrodes implanted into muscles, two on each side. Our intention was to target the pectoralis major (PM) and the pronator superficialis (PS) on both the left and right sides. The PM was targeted because it powers the downstroke and its activity varies in response to mechanical demands (Hagiwara et al., 1968; Altshuler et al., 2010; Tobalske et al., 2010). The PS was targeted because it is one of the larger superficial muscles in the hummingbird wing (Welch and Altshuler, 2009). It is nonetheless a very small muscle and we inadvertently recorded from two other proximal wing muscles, the pronator profundus (PP) and the flexor digitorium superficialis (FDS) in place of recordings intended from the PS.

The EMG wires were made of 99.99% silver with heavy polyimide (HML) insulation (California Fine Wire, Grover Beach, CA, USA). The vendor fabricated electrically isolated wire pairs ('bifilar') made of either 0.0508 or 0.0762 mm diameter wires. We used the 0.0508 mm electrodes with the proximal wing muscles (FDS, PP and PS), and the 0.0762 mm electrodes with the PM. A single 0.1016 mm silver wire, also insulated with HML, served as the ground electrode. We removed the last 0.5 mm of insulation from the end of each wire, and offset the ends of the paired wires by 0.5 mm.

To secure the electrodes around the muscle fibers, we fed the end of the wire or wire pair into the tip of a hypodermic needle and then bent back the wire to form a hook. We then inserted the recording electrodes into the muscles and the ground electrode subcutaneously on the back above the vertebral column using the needle. We removed the needle and left the wires in place by holding it with forceps as the needle was removed. The electrodes were secured with 6-0 sutures to the skin of the hummingbird over the site of insertion and we additionally secured the full set of lead wires with suture through the intervertebral fascia.

Following recovery from the initial surgery, hummingbirds were released in the flight chamber. Three different flight behaviors were recorded: stationary hovering, clockwise turning and counterclockwise turning. All recordings with the revolving feeder were made at 30 r.p.m. Two trial recordings of each flight behavior were made for each bird with one exception: only one trial was made for bird 4 during hovering. The trials and behaviors were varied in temporal sequence. A trial was considered successful if the bird fed from the feeder for at least 0.5 s. Trials were separated by 20 min and all the trials for each bird were recorded in a single day. Following data collection, each bird was briefly anesthetized with isoflurane and the electrodes were removed, taking care to prevent damage to muscle fibers. The body mass was recorded on a digital scale and the wings on both sides of the bird were photographed in an outstretched position against white paper with a reference scale. Measurements of wing length, wing area, aspect ratio and the non-

dimensional moments of wing area were calculated using custom analysis software in MATLAB (The MathWorks, Natick, MA, USA).

### Electromyography

EMG signals from the electrodes were amplified ×1000 using a multi-channel extracellular amplifier (model 1700, A-M Systems, Sequim, WA, USA), with the low- and high-frequency cut-offs of the online filters set at 0.1 Hz and 10 kHz, respectively. The amplifier output was acquired at 10,000 samples $s^{-1}$ (0.1 ms resolution) with an analog-to-digital acquisition board (Digidata 1440, Molecular Devices, Sunnyvale, CA, USA). The electrophysiology data were synchronized with the high-speed cameras (1 ms resolution) by recording the camera trigger pulse with the acquisition system.

The EMG signals were filtered offline using zero-phase, fourth-order high-pass Butterworth filters with cut-off frequencies set between three and 12 times the wingbeat frequency. The wing strokes were defined by the furthest angular extents within the stroke plane to determine the relative timing of excitation events. All EMG analyses were performed separately for the left and right wings because the angular extreme sometimes occurred at different times.

The muscle activation timing and intensity were examined using different representations depending upon the muscle (Table 1). The PM is unusual in having a relatively small number of discrete excitation waveforms, and the spike amplitudes are correlated with wingbeat kinematics and flight speeds (Hagiwara et al., 1968; Altshuler et al., 2010; Tobalske et al., 2010). We accordingly used the occurrence of the first spike ($\dot{t}$) as the measure of activation timing relative to the wingbeat, and the normalized maximum spike amplitude ($\hat{E}_{max}$) as the measure of activation intensity. The proximal wing muscles have more typical vertebrate activation patterns in that the burst duration is longer and a greater number of waveforms are present. We accordingly used the average spike occurrence ($\bar{t}$) relative to the wingbeat for activation timing, and the normalized, rectified area of the waveform ($\hat{E}_{area}$) as the measure of activation intensity. The timing and activation variables were calculated over a wingbeat cycle beginning and ending at the upstroke–downstroke transition (pronation) for the PM and PS. The wingbeat cycle for the PP began and ended at the downstroke–upstroke transition (supination). Because the PP and PS have biphasic activation patterns, we analyzed the first and second bursts independently. We recorded the FDS from only one side of one animal, which was insufficient to include its excitation features in the analysis. We normalized both measures of EMG intensity by first calculating the log of each variable per wingbeat cycle and then confirming that the maximum value was not an outlier. All of the intensity measures for a single electrode were then divided by the maximum value for that electrode.

Table 1. Variables used to describe the kinematic and electromyographic features of hovering and yaw turns in hummingbirds

| Variable | Symbol |
|---|---|
| Electromyographic features | |
| Normalized maximum spike amplitude | $\hat{E}_{max}$ |
| Normalized rectified area | $\hat{E}_{area}$ |
| Time of the first spike | $\dot{t}$ |
| Average spike time | $\bar{t}$ |
| Kinematic features | |
| Yaw angle | $\Psi$ |
| Wingtip speed | $U_{tip}$ |
| Body angle, lateral | $\chi_{GR,XZ}$ |
| Body angle, frontal | $\chi_{GR,YZ}$ |
| Position angle | $\phi_{GR}$ |
| Elevation angle | $\theta_{GR}$ |
| Average elevation angle | $\bar{\theta}_{GR}$ |
| Stroke plane angle | $\beta$ |
| Stroke amplitude | $\Phi_{SP}$ |
| Elevation amplitude | $\Theta_{SP}$ |

Kinematic variables were calculated separately for each downstroke and upstroke. Electromyographic variables were calculated over the wingbeat, which included two distinct bursts for the pronator profundus and pronator superficialis muscles.

### Kinematic digitization

High-speed images of each hummingbird flying in the cage were recorded in three views by two cameras. One camera (Troubleshooter, Fastec Imaging, San Diego, CA, USA) recorded at 640×480 pixel resolution through a mirror placed at an angle of 45 deg under the chamber, providing the bottom view of the hummingbird. A second camera (Miro 4, Vision Research, Wayne, NJ, USA) recorded the front view and a side view. The side view was filmed through a second mirror placed outside the left wall of the chamber and tilted at an angle of 45 deg. This camera recorded both perspectives using an aspect ratio and resolution of 800×600 pixels. Both cameras filmed at 1000 frames $s^{-1}$ with a shutter speed of 1/5000 s. The image sequences in both cameras terminated with a common end trigger, thereby synchronizing the videos.

The three camera views were calibrated using the direct linear transformation (DLT) technique with a 14-point calibration frame and DLTdv3 software (Hedrick, 2008). Six points were digitized on each hummingbird: left wing tip, right wing tip, right shoulder, left shoulder, top of the head and the tip of the middle tail feather. Every third frame in each video was digitized, and the resulting data were fit with a cubic spline to extrapolate the points in the remaining frames. These splined 2-D points were then checked and refined frame-by-frame within DLTdv3. After the 2-D points were refined, the 3-D real-world body points were filtered with zero-phase, fourth-order low-pass Butterworth filters. The filter cut-off frequencies ranged between 1.5 and 5 times the wingbeat frequency, with generally lower cut-off frequencies for the head position and higher cut-off frequencies for the tail, wing shoulder and wingtip positions.

The images were sampled at 1000 frames $s^{-1}$, which translated to ~25 frames $wingbeat^{-1}$ or ~25 time points per wing and body point. To improve the estimate of the maximum and minimum excursions and their phasing with respect to EMGs, the filtered kinematic data were upsampled to 10,000 frames $s^{-1}$ and fit with a cubic spline using the interpolate package from the Scientific Tools for Python (SciPy) module (Python Software Foundation, Wilmington, DE, USA). This procedure increased precision in the calculation of wing angles, stroke duration and muscle activation phase relative to wing motion. The pronation time for each wing was defined as the time of the minimum excursion in the stroke plane whereas the supination time was defined by the maximum excursion. The pronation and supination times were used to calculate the wing stroke durations and the relative timings of the muscle activation features.

### Frame of reference and coordinate system

We compared the kinematics across wingbeats using two frames of reference, both defined in part by the position of the wings at the start and end of each downstroke and upstroke (Fig. 1B). We used wing-stroke-centered frames of reference because the tail exhibited

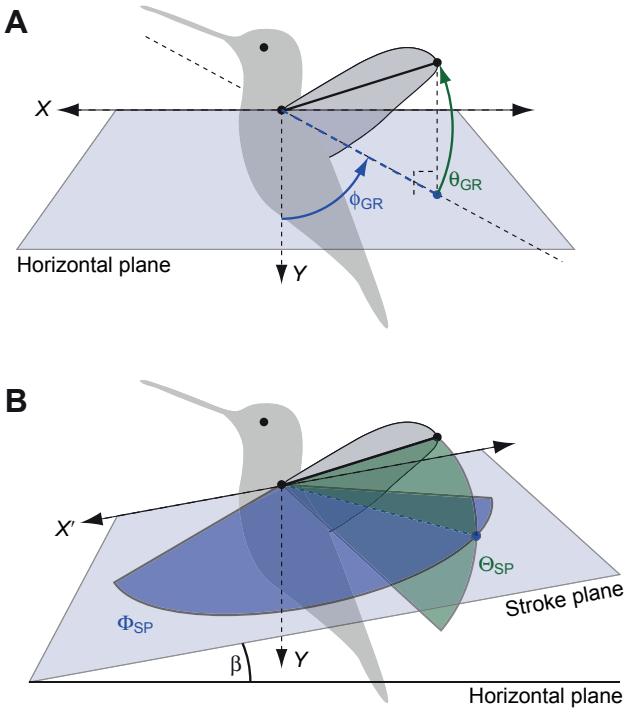


Fig. 2. Within the gravitational frame of reference, the wing elevation angle ($\theta_{GR}$) and stroke position angle ($\phi_{GR}$) were calculated for each image frame (A). The stroke plane frame of reference was shifted by the stroke plane angle ($\beta$), and the elevation amplitude ($\Theta_{SP}$) and stroke amplitude ($\Phi_{SP}$) were calculated once per stroke (B).

high-frequency oscillations (Altshuler et al., 2009) and the body position varied within and among trials. One frame of reference was constrained by gravity and other was aligned with the stroke plane.

In the gravitational frame of reference (Fig. 2A), the *Z*-axis was set parallel to gravity, thereby defining an *X*–*Y* plane parallel to the ground. Each wing stroke was rotated about the *Z*-axis by defining the *X*-axis as a line located in between the left and right wingtip paths projected into the *X*–*Y* plane. The midpoints between the wingtips at the upstroke–downstroke transition and downstroke–upstroke transition were used to calculate the wingtip path dividing line. Thus, the frame of reference rotated for each stroke, and kinematic parameters were calculated for downstroke and upstroke separately. The yaw angle $\Psi$ was defined as the angular rotation between strokes (Fig. 1B), and the number of values per trial was therefore twice the number of wingbeats. Within the gravitational frame of reference, positive *Z* was towards the sky and the bird faced the positive direction of the *X*-axis. This frame of reference allowed us to maintain the aerodynamic relevance to gravity but still compare the paths of each individual wing strokes.

The stroke-plane-centered frame of reference (Fig. 2B) differed from the gravitational frame of reference in two respects: (1) the *Z*′-axis was orthogonal to the stroke plane and (2) the stroke planes, and therefore the frames of reference, were calculated separately for the left and right wings. This transformation allowed for comparison of the deviations from the stroke plane between the left and right wings, across wingbeats and among animals.

### Kinematic variables

We defined 10 kinematic variables, which were calculated separately for each downstroke and upstroke (Table 1). Yaw angle was described above for the frames of reference. Six variables were calculated in the gravitational frame of reference. The wingtip speed $U_{tip}$ was calculated by dividing the distance traveled through the three dimensions by the duration of the stroke. The body axis was defined as a line through the head and tail, and its orientation with respect to the horizontal plane and the bird's orientation provided two body angles. The lateral body angle $\chi_{GR,XZ}$ was calculated in the *X*–*Z* plane and the frontal body angle $\chi_{GR,YZ}$ was calculated in the *Y*–*Z* plane.

Two wing angles were calculated for each time step with respect to gravity. The instantaneous position angle $\phi_{GR}$ describes the angle between the shoulder to wingtip vector and the *Y*-axis, projected into the *X*–*Y* plane (Fig. 2A). The values are constrained between –90 deg (directly behind the bird) and +90 deg (directly in front of the bird). The instantaneous elevation angle $\theta_{GR}$ describes the angle between the shoulder to wingtip vector and its projection in the *X*–*Y* plane. Its values are constrained between –90 deg (directly below the bird) and +90 deg (directly above the bird). The average of the elevation angle for each stroke $\bar{\theta}_{GR}$ provides the position of the stroke plane relative to the shoulder.

The stroke plane was determined using reduced major axis (RMA) regression of the wingtip positions in the *X*–*Z* plane for each wing in each stroke. The stroke plane angle $\beta$ is the angle between the slope of the RMA regression and the horizontal plane (Fig. 2B). Negative values indicate that the beginning of the stroke is at a higher elevation than the end of the stroke. The wing stroke amplitude $\Phi_{SP}$ is the angle from the rearward most position of the wingtip to the shoulder to the forward most position of the wingtip, projected into the stroke plane. The elevation amplitude $\Theta_{SP}$ is the sum of the

Table 2. Morphological parameters of the four male Anna's hummingbirds (*Calypte anna*) used in the study

| Bird | *M* (g) | Side | *R* (mm) | *S* (mm$^2$) | AR | $\hat{r}_1(S)$ | $\hat{r}_2(S)$ | $\hat{r}_3(S)$ |
|---|---|---|---|---|---|---|---|---|
| 1 | 4.20 | Left | 48.66 | 1323.70 | 7.16 | 0.4332 | 0.5101 | 0.5643 |
| | | Right | 46.25 | 1098.30 | 7.79 | 0.4061 | 0.4816 | 0.5368 |
| 2 | 4.21 | Left | 50.43 | 1247.30 | 8.16 | 0.4117 | 0.4850 | 0.5377 |
| | | Right | 52.68 | 1389.30 | 7.99 | 0.4243 | 0.4998 | 0.5535 |
| 3 | 4.06 | Left | 50.51 | 1270.40 | 8.03 | 0.4241 | 0.5023 | 0.5579 |
| | | Right | 51.18 | 1378.90 | 7.60 | 0.4395 | 0.5150 | 0.5692 |
| 4 | 4.64 | Left | 47.56 | 1165.20 | 7.76 | 0.4258 | 0.5003 | 0.5537 |
| | | Right | 51.26 | 1402.90 | 7.49 | 0.4354 | 0.5101 | 0.5636 |

Body mass (*M*) is the mean of measurements taken before and after each trial. The wing size parameters, wing length (*R*) and wing area (*S*), as well as the wing shape parameters of aspect ratio (AR) and non-dimensional radii of the first [$\hat{r}_1(S)$], second [$\hat{r}_2(S)$] and third [$\hat{r}_3(S)$] moments of wing area were calculated from a digital photograph of a single wing. The wing area and aspect ratio are calculated for two wings to allow for comparisons with other measurements of hovering animals (Ellington, 1984).

maximum and minimum angles, each defined as an angle between the shoulder to wingtip vector and its projection into the stroke plane. The frame of reference transformations and the calculations of the kinematic variables were made using custom software written in Python (Python Software Foundation).

### Statistical analysis

Sequences of wingbeat kinematics and muscle activations represent time series data. We used four statistical approaches to analyze how these variables changed across flight modes. All statistical analyses were implemented in R (R Development Core Team, 2012).

The variation in the kinematic and EMG variables by flight mode was compared using the intra-class correlation coefficient (ICC), which is the most common measure of repeatability. The specific method was ANOVA-based (Lessells and Boag, 1987; Whitlock and Schluter, 2009). The EMG values were considered separately for the left and right sides. The kinematic values were assessed for left-right differences for the downstrokes and upstrokes separately. The two trials of each flight mode were combined for ICC analysis.

To examine overall changes in mean values of kinematic and EMG parameters, we employed a mixed-model ANOVA with flight mode (hover, clockwise and counterclockwise) as the fixed effect and bird as a random effect. For kinematic variables, downstroke and upstroke were separated. The ANOVA approach led to a massive reduction in the data set, utilizing a mean value for each measure for each bird per flight mode. We chose to use a single mean instead of a more complicated mixed-model ANOVA (e.g. trial nested within bird), because of low variance within measures per bird–flight-mode combination. For models with significant overall ANOVAs ($\alpha<0.05$), a *post hoc* analysis was employed to test for significant differences between clockwise and hovering and between counterclockwise and hovering using general linear hypothesis tests corrected for multiple comparisons (Hothorn et al., 2008).

The third approach was to use time series analysis to consider how the relationships between kinematic and EMG measures changed through time. We first calculated the autocorrelation, which is the cross-correlation of each individual measure with a 32-time point (i.e. 16 downstroke–upstroke pairs), time-lagged version of itself (Venables and Ripley, 2002). Using a similar approach, we then examined cross-correlations among pairwise combinations of all variables (kinematic *versus* kinematic and kinematic *versus* electromyographic) for the same 16 wingbeats. Because the sequences of wingbeats were too short for standard time series detrending procedures, which are used to remove non-stationarity from time series data (Cowpertwait and Metcalfe, 2009), we implemented a method based on linear regression. We first determined the ordinary least-squares regression slope of each observation of each variable *versus* time (wing stroke period 1–32). We then used the 2-D rotation matrix to rotate the data so that the new slope was zero.

We assessed significance of autocorrelation analyses by aggregating the proportion of each measure with at least one non-zero lag value whose correlation fell outside a 95% confidence interval for autocorrelation. We used only non-zero lags because the correlation at lag=0 is 1 by definition and, thus, is always significant. Significance among cross-correlation analyses was assessed *via* randomization. For each set of variables (kinematic *versus* kinematic and kinematic *versus* EMG), we generated a null distribution for each variable for each of lags=–2, –1, 0, 1 and 2. This range of lags corresponds to a period including synchronous correlation (lag=0) as well as correlations of ±½ and ±1 wingbeat. An analytical *P*-value for each variable–lag combination was determined as the median of the proportion of times that the observed cross-correlation exceeded the randomized cross-correlation. Because checking over 1000 distributions for normality was impractical, we chose to use the median, which is a better estimator of central tendency for skewed distributions and converges on the mean for normally distributed samples. This method produced more conservative results than assessing the likelihood of significance based on the percentage of significant cross-correlation analyses for each variable–lag combination.

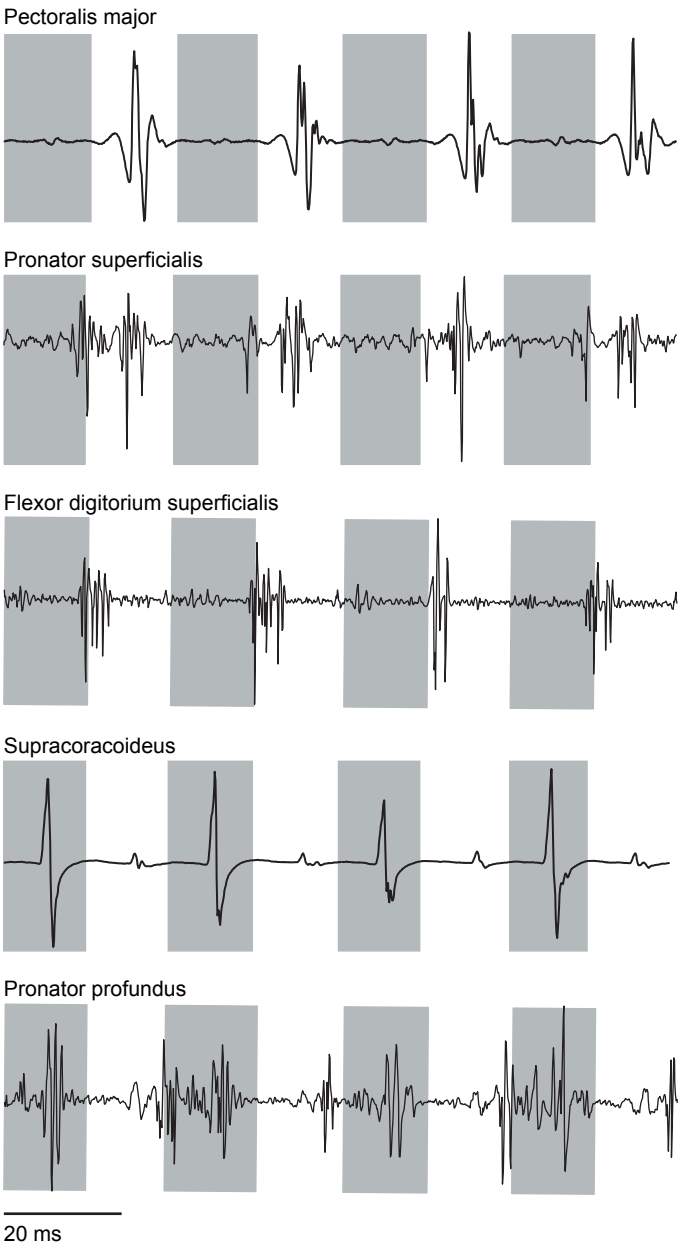


Fig. 3. Raw electromyogram recordings from five flight muscles in *Calypte anna*. The signals were acquired with the online analog filers wide open and are presented without post-processing. Four wing strokes are depicted for each muscle. Downstrokes are indicated by gray bars and upstrokes are in white. The voltage increments of the *y*-axis have been scaled for each panel so that each muscle trace spans the same range. The recordings come from different individuals but the time scale is the same for all traces. The recordings of the pectoralis major, pronator superficialis, pronator profundus and flexor digitorium superficialis come from the present study. A verified recording of the supracoracoideus using identical methods but from a different individual is also included.

Table 3. Average wingbeat frequencies (*f*, Hz) and stroke amplitude differences ($\Delta\Phi$; deg) for four adult male Anna's hummingbirds (*C. anna*) during hovering and turning

| | Clockwise | | | | Hovering | | | | Counterclockwise | | | |
|---|---|---|---|---|---|---|---|---|---|---|---|---|
| Bird | *N* | *f* | $\Delta\Phi_{DS}$ | $\Delta\Phi_{US}$ | *N* | *f* | $\Delta\Phi_{DS}$ | $\Delta\Phi_{US}$ | *N* | *f* | $\Delta\Phi_{DS}$ | $\Delta\Phi_{US}$ |
| 1 | 38 | 41.59 | 0 | –8.46 | 33 | 40.54 | –2.52 | –1.61 | 32 | 39.88 | –15.03 | –6.39 |
| 2 | 32 | 39.49 | 14.75 | 6.07 | 32 | 39.63 | 3.32 | 4.10 | 44 | 39.76 | 2.21 | 8.75 |
| 3 | 32 | 39.81 | –5.85 | –10.85 | 33 | 39.69 | –12.46 | –12.03 | 33 | 40.58 | –13.91 | –6.58 |
| 4 | 31 | 37.7 | 6.09 | –2.44 | 30 | 36.84 | –4.44 | –4.75 | 15 | 36.76 | –7.21 | –0.33 |

The number of wing strokes (*N*) is provided by bird and treatment. The stroke amplitudes are presented as left minus right differences for the downstroke (DS) and upstroke (US). Statistical analysis of the wingtip speed and stroke amplitude is provided in Table 7.

The fourth approach, principal components analysis (PCA), was carried out to confirm the results of the ANOVA and cross-correlation analyses among kinematic variables only. Because of the incomplete nature of the EMG data, these data could not be included in the PCA analysis. All variables were scaled to unit variance prior to the analysis.

## RESULTS

The body mass and wing morphology of the four *C. anna* used in experiments are given in Table 2. Separate measurements were made on the left and right wings and paired *t*-tests were used to determine whether the wing morphology variables differed by side. Although there were small asymmetries for each of the wing variables, there was no systematic difference by side (all $P>0.45$).

Representative EMGs are provided in Fig. 3. These raw recordings were made with the online analog filters wide open and have not been post-processed. The signals come from different individuals during hovering flight. The PM and the three wing muscles (FDS, PP and PS) come from the birds in the present study. A verified recording from the SC of a different individual adult male *C. anna* is also presented for comparison. Other than electrode placement, the SC recording was made using methods identical to those used for the PM recordings.

The PM becomes active midway through the upstroke and likely generates muscle force at stroke transition and during the subsequent downstroke. The PS and FDS become active at the downstroke–upstroke transition and presumably generate force during the latter half of the upstroke, possibly continuing through stroke transition. The FDS was not recorded with sufficient sample size for analysis but it is included here because the position of the electrode that recorded this trace was confirmed post mortem. The SC becomes active midway through the downstroke and likely generates muscle force at stroke transition and during the subsequent upstroke. The PP becomes active during the upstroke–downstroke transition and probably generates force during the latter half of the downstroke, continuing through stroke transition.

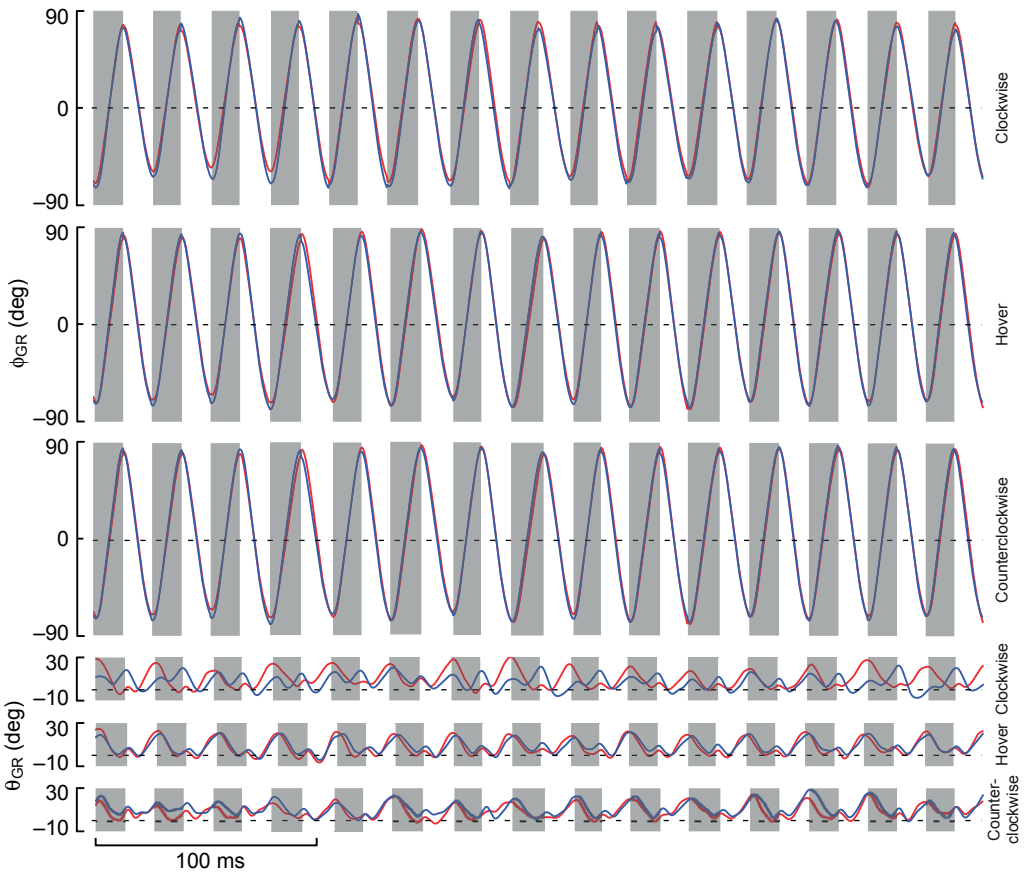


Fig. 4. Representative traces in the gravitational frame of reference. The position angle $\phi_{GR}$ and elevation angle $\theta_{GR}$ are presented for 15 wingbeats across three trials, one each of clockwise, hovering and counterclockwise flight. The left wing is indicated in red and the right wing is indicated in blue. Downstrokes are shaded in gray and upstrokes are in white. Discontinuities between strokes result from shifts in the frame of reference.

Table 4. The intra-class correlation coefficients (ICCs) for the intensity and timing measures of the pectoralis major, pronator profundus and pronator superficialis muscles during hovering, and clockwise and counterclockwise yaw turns

| Maneuver | Intensity | Timing |
|---|---|---|
| Pectoralis major | | |
| Clockwise | 0.19 | 0.52 |
| Hovering | 0.43 | 0.51 |
| Counterclockwise | 0.41 | 0.35 |
| Pronator profundus | | |
| Clockwise | 0.15 | 0.79 |
| Hovering | 0.35 | 0.82 |
| Counterclockwise | 0.26 | 0.49 |
| Pronator superficialis | | |
| Clockwise | 0.23 | 0.52 |
| Hovering | 0.01 | 0.74 |
| Counterclockwise | 0.40 | 0.55 |

The left and right sides were calculated separately for the pectoralis major and the average values are presented here. Only one side was available for each of the pronator profundus and pronator superficialis.

Table 5. Intra-class correlation coefficients (ICCs) for whole-body kinematic features, yaw angle ($\Psi$) and body kinematics (lateral body angle, $\chi_{GR,XZ}$, and frontal body angle, $\chi_{GR,YZ}$), and for left–right wing kinematics, wingtip speed ($U_{tip}$), average elevation angle ($\bar{\theta}_{GR}$), stroke plane angle ($\beta$), stroke amplitude ($\Phi_{SP}$) and elevation amplitude ($\Theta_{SP}$)

| | Clockwise | Hovering | Counterclockwise |
|---|---|---|---|
| $\Psi_{DS}$ | –0.01 | –0.01 | 0.01 |
| $\Psi_{US}$ | –0.03 | –0.02 | –0.02 |
| $\chi_{GR,XZ,DS}$ | 0.37 | 0 | 0.08 |
| $\chi_{GR,XZ,US}$ | 0.34 | 0.11 | 0.08 |
| $\chi_{GR,YZ,DS}$ | 0.60 | 0.19 | 0.39 |
| $\chi_{GR,YZ,US}$ | 0.58 | 0.17 | 0.30 |
| $U_{tip,DS}$ | 0.68 | 0.78 | 0.62 |
| $U_{tip,US}$ | 0.58 | 0.75 | 0.55 |
| $\bar{\theta}_{GR,DS}$ | 0.48 | 0.70 | 0.62 |
| $\bar{\theta}_{GR,US}$ | 0.60 | 0.59 | 0.54 |
| $\beta_{DS}$ | 0.50 | 0.17 | 0.45 |
| $\beta_{US}$ | 0.61 | 0.53 | 0.42 |
| $\Phi_{SP,DS}$ | 0.62 | 0.61 | 0.59 |
| $\Phi_{SP,US}$ | 0.49 | 0.60 | 0.48 |
| $\Theta_{SP,DS}$ | 0.16 | 0.16 | 0.17 |
| $\Theta_{SP,US}$ | 0.30 | 0.05 | 0.09 |

The upstrokes and downstrokes were analyzed separately.

The revolving feeder had a constant rotation of 30 r.p.m., but the hummingbirds did not track the feeder with constant angular velocity and instead varied the yaw angles by stroke (Fig. 1C). The maximum angular changes in left (counterclockwise, –7.9 deg) and right (clockwise, 11.4 deg) yaw angle were recorded during downstrokes. The birds exhibited small changes in yaw during hovering (blue traces) at a stationary feeder.

The average wingbeat frequencies and left–right differences in stroke amplitude are given for the four individuals in Table 3. Among individuals, wingbeat frequencies varied as much as 4 Hz within a flight mode, but within individuals this value was less than 1 Hz across the three flight modes. The differences in left–right stroke amplitude were similar between upstroke and downstroke for each individual during hovering flight. The values for clockwise flight were always more positive for the downstroke, whereas the counterclockwise values were more positive for the upstroke. Thus, the outer–inner difference in stroke amplitude was consistently higher on the downstroke compared with the upstroke.

The instantaneous wing position angles in the gravitational frame of reference were sinusoidal and highly repeatable for both wings across wingbeats for all three treatments (Fig. 4). The instantaneous elevation angles were also similar between left and right wings, and across wingbeats during hover feeding. However, these traces were much more variable during clockwise and counterclockwise feeder tracking. In these cases, the left and right wings exhibited divergent patterns that also varied considerably across wingbeats.

### Intra-class correlation

The ICC or repeatability values for the timing and intensity features of the PM, PP and PS are provided in Table 4. Across all muscles and flight modes, the mean ICC for the timing features ($\bar{x}$=0.59) is higher than for the intensity features ($\bar{x}$=0.27). During hovering flight, the repeatability of the timing features is higher or nearly so compared with the other flight modes. For the intensity features, the repeatability values for the PM were generally higher or nearly so compared with the other two muscles.

The ICC values for the kinematic variables spanned a wide range (Table 5). The negative values arise when there is greater variability within than among individuals. However, it has been suggested that this situation is unlikely to occur in nature and that negative values represent statistical noise around what is effectively zero repeatability (Nakagawa and Schielzeth, 2010). The most consistently low values were for the yaw angles during both strokes, further demonstrating that the hummingbird tracked the revolving feeder with high variation across strokes. The stroke amplitudes and the wingtip velocities exhibited relatively high repeatability for both strokes across all three maneuvers. This was also the case for the average elevation angle, but the ICC values for the elevation amplitude were relatively low. The body angles and stroke plane angles exhibited a broader range in ICC values.

Table 6. Mixed-model ANOVA of yaw angle ($\Psi$) and body kinematics (lateral body angle, $\chi_{GR,XZ}$, and frontal body angle, $\chi_{GR,YZ}$) by maneuver

| Variable | d.f. | $F$ | $P$ | $P_{ck\text{-}hv}$ | $P_{ct\text{-}hv}$ |
|---|---|---|---|---|---|
| $\Psi_{DS}$ | 2,6 | 225.84 | <0.0001 | <0.0001 | <0.0001 |
| $\Psi_{US}$ | 2,6 | 521.79 | <0.0001 | <0.0001 | <0.0001 |
| $\chi_{GR,XZ,DS}$ | 2,6 | 3.95 | 0.0804 | | |
| $\chi_{GR,XZ,US}$ | 2,6 | 4.23 | 0.0714 | | |
| $\chi_{GR,YZ,DS}$ | 2,6 | 1.41 | 0.3143 | | |
| $\chi_{GR,YZ,US}$ | 2,6 | 1.41 | 0.3155 | | |

Bird was included as a random effect within the model. Two *post hoc* comparisons were made for models with significant ANOVAs: clockwise *versus* hovering (ck-hv) and counterclockwise *versus* hovering (ct-hv).

Table 7. Mixed-model ANOVA of wingbeat kinematics: wingtip speed ($U_{tip}$), average elevation angle ($\bar{\theta}_{GR}$), stroke plane angle ($\beta$), stroke amplitude ($\Phi_{SP}$) and elevation amplitude ($\Theta_{SP}$)

| Variable | d.f. | $F$ | $P$ | $P_{ck\text{-}hv}$ | $P_{ct\text{-}hv}$ |
|---|---|---|---|---|---|
| $U_{tip,DS}$ | 2,6 | 4.00 | 0.0786 | | |
| $U_{tip,US}$ | 2,6 | 4.80 | 0.0570 | | |
| $\bar{\theta}_{GR,DS}$ | 2,6 | 70.71 | <0.0001 | <0.0001 | 0.0007 |
| $\bar{\theta}_{GR,US}$ | 2,6 | 10.46 | 0.0111 | 0.0074 | 0.1833 |
| $\beta_{DS}$ | 2,6 | 2.00 | 0.2155 | | |
| $\beta_{US}$ | 2,6 | 6.42 | 0.0323 | 0.0384 | 0.3734 |
| $\Phi_{SP,DS}$ | 2,6 | 17.58 | 0.0031 | 0.0005 | 0.0485 |
| $\Phi_{SP,US}$ | 2,6 | 1.31 | 0.3383 | | |
| $\Theta_{SP,DS}$ | 2,6 | 23.28 | 0.0015 | <0.0001 | 0.1100 |
| $\Theta_{SP,US}$ | 2,6 | 11.84 | 0.0083 | 0.0008 | 0.4128 |

Two *post hoc* comparisons were made for models with significant ANOVAs: clockwise *versus* hovering (ck-hv) and counterclockwise *versus* hovering (ct-hv). Other details as in Table 4.

### Mixed-model ANOVA

The mixed-model ANOVAs revealed broad patterns of differences in mean kinematic measures across flight maneuvers (Tables 6, 7) with no significant differences in EMG measures (all $P$>0.2). Significant differences were found among flight modes in yaw angle ($\Psi$), average elevation angle ($\bar{\theta}_{GR}$) and elevation amplitude ($\Theta_{SP}$) for both upstroke and downstroke, stroke plane angle ($\beta$) during upstroke, and stroke amplitude ($\Phi_{SP}$) during downstroke. Based on *post hoc* tests comparing clockwise and counterclockwise maneuvers with hovering, clockwise maneuvers are more different from hovering than are counterclockwise maneuvers. The kinematic variable with the strongest differences between hovering and yaw maneuvers is $\bar{\theta}_{GR}$. The complete data set for this variable during the downstroke as well as several other kinematic and EMG variables is provided in Fig. 5. In addition to wingbeat- and stroke-specific values, these plots contain the mean values by bird and

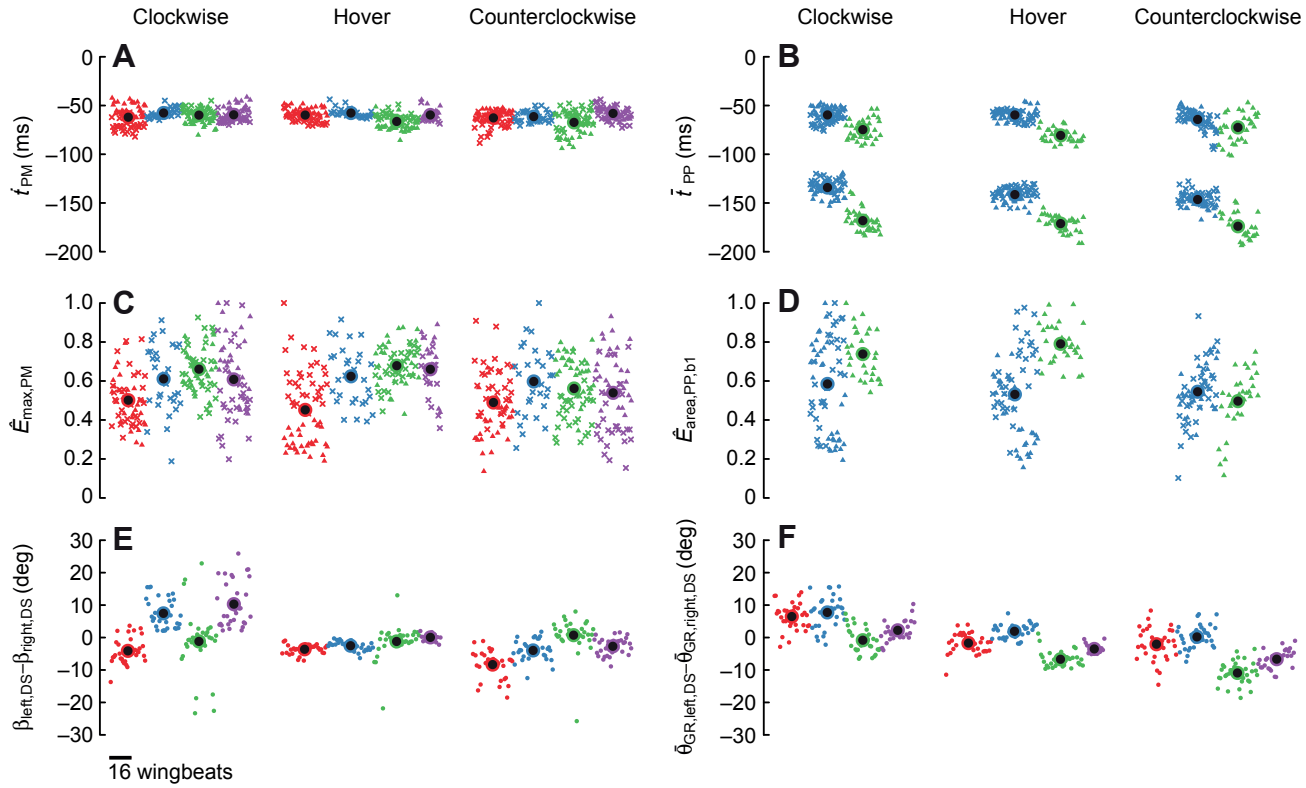


Fig. 5. Representative electromyographic (EMG) and kinematic variables through time. The data are presented from left to right in order (within each trial) as the individual wingbeats or strokes with trial 1 preceding trial 2. The scale bar represents the length of most of the trials. The colors indicate the four individuals in the study (red, bird 1; blue, bird 2; green, bird 3; purple, bird 4). For the EMG variables (A–D), triangles indicate the muscles of the right wing and crosses indicate the muscles of the left wing. For the kinematic variables (E,F), filled circles represent the left minus right values. The timing values for the pectoralis major (PM) (A) and both bursts of the pronator profundus (PP) (B) are the first spike time ($\dot{t}$) and the average spike time of each burst ($\bar{t}$), respectively. The intensity values for the PM (C) and the first burst of the PP (D) are the normalized maximum spike amplitude ($\hat{E}_{max}$) and the rectified area of the waveform ($\hat{E}_{area}$), respectively. The representative kinematic variables are the difference in the stroke plane angle ($\beta$; E) and average elevation angle ($\bar{\theta}_{GR}$; F) during downstrokes. All wingbeats (A–D) and downstrokes (E,F) were used for the time series analysis, but the mixed-model ANOVAs included only the averages by bird and maneuver (large circles with black centers).

maneuver, which are the inputs to the mixed-model ANOVAs. This approach clearly eliminates time-varying patterns of potential interest for understanding flight control.

### Time series analysis

A large number of variables had at least one non-zero lag correlation that fell outside a 95% confidence interval (supplementary material Table S1). The muscle activation features were autocorrelated in 43% of all trials. Kinematic variables were autocorrelated in 71% of the trials, and some variables, such as body angles, average elevation angles, elevation amplitudes and stroke plane angles, were autocorrelated in almost every trial. Two general patterns of autocorrelation are present: (1) sinusoidal autocorrelation at low frequencies, which characterize changes in body angles, and (2) alternating autocorrelation, corresponding to differences between upstrokes and downstrokes, which characterize stroke plane angle, elevation angle, elevation amplitude and wingtip speed (Fig. 6).

There are a large number of cross comparisons among kinematic and EMG variables. The cross-correlation analysis between kinematics and EMGs is composed of 800 variable combinations with a sample size of 8640 for all four individuals. Comparisons within kinematics are composed of 280 variable combinations with a sample size of 6440. When analyzed without correcting for multiple comparisons, many of the kinematic and EMG combinations appear to show significant cross-correlation, e.g. the average time of the first burst of the PS with kinematic measures at multiple lags (supplementary material Fig. S1). However, subsequent randomization analysis demonstrated that significant cross-correlation is highly probable for randomly ordered data, resulting in no significant $P$-values across all 800 comparisons ($P$>0.06; supplementary material Fig. S2). Patterns of cross-correlation among kinematic measures are widespread, both considering percentage significant (supplementary material Fig. S3) and $P$-value *via* randomization (Fig. 7). Significant cross-correlations at lags ±½ and ±1 wingbeat are widespread among kinematic measures. The strongest ($P$<0.005) and most consistent (present on both sides) cross-correlations were between average elevation angle and elevation amplitude, and between stroke amplitude and wingtip speed, all at zero lag.

### Principal components analysis

Principal components analysis showed kinematic measures to co-vary largely independently of one another (supplementary material Fig. S3, Table S2). Only yaw angle ($\Psi$) and frontal body angle ($\chi_{GR,XZ}$) loaded similarly on the first and second PCs. All other variables loaded differently from each other on the first two PCs. In contrast to most PCAs, the proportion of variance accounted for by the first two PCs was just over half.

## DISCUSSION

### Overall kinematic changes

Hummingbirds sustain yaw turns using two distinct kinematic mechanisms: (1) extending the stroke amplitude of the outer wing during the downstroke, and (2) substantially altering the deviation path of both wings during both strokes. For the first mechanism, it is important to note that our frames of reference are set by the extreme positions of the wing strokes. The feeder revolved at an angular rate of ~4.5 deg per wingbeat or ~2.25 deg per wing stroke given the near-constant wingbeat frequency. If a hummingbird tracked the feeder at the same rate while using a constant stroke amplitude with respect to its body, its expected left–right stroke amplitude difference was 4.5 deg per stroke or 9.0 deg per wingbeat. During clockwise turns, the average left–right stroke amplitude during the downstroke was 3.75 deg, and during counterclockwise turns, the average value was –8.49 deg. During hovering, the average downstroke value was –4.02 deg, which was significantly different from the values exhibited during turning (Table 7). Because the measured values fall close to or within the range of the expected values during turns, it is not known the extent to which the asymmetry in stroke amplitudes was a cause or a consequence of yaw torque. The asymmetries are nonetheless a relevant feature given that variation in wing stroke amplitude is one of the primary

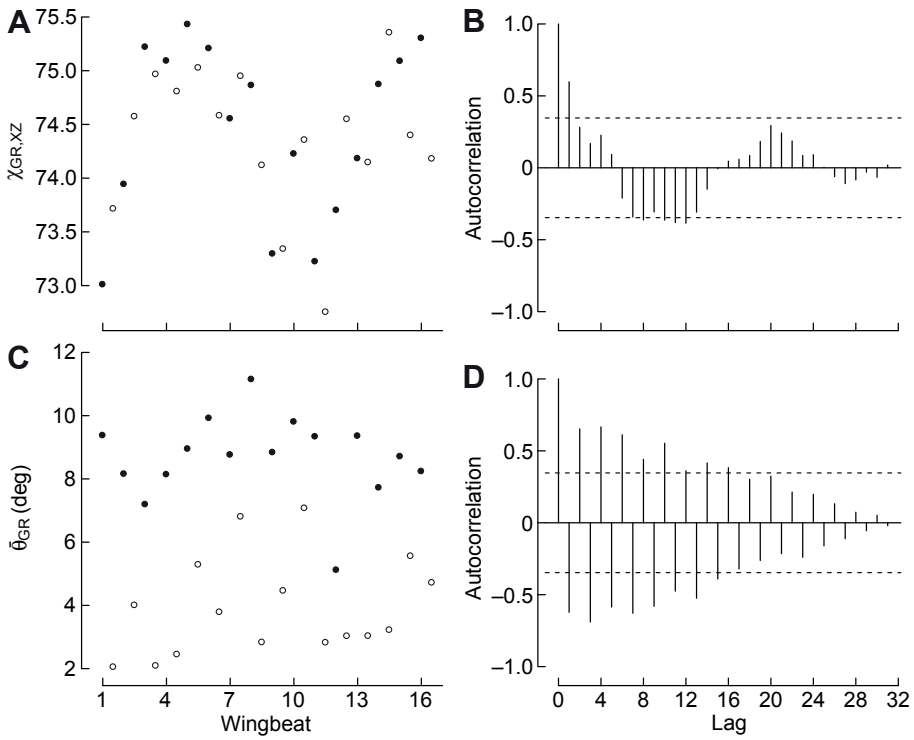


Fig. 6. Representative autocorrelation functions. The change in kinematic variables through time are provided for the lateral body angle (A) and average elevation angle on the right wing (C) during the first hovering trial of bird 2. The downstrokes are indicated by filled circles and the upstrokes are indicated by unfilled circles. The corresponding autocorrelations are provided on the right (B,D). The autocorrelation lags are defined per stroke. In general, significant autocorrelations for the body angles consisted of sinusoidal time series, and significant autocorrelations for the wing angles consisted of alternative times series for the downstrokes and upstrokes.

| Lag | $\chi_{GR,YZ}$ | $\chi_{GR,XZ}$ | $\Theta_{SP}$ | $\Phi_{SP}$ | $\beta$ | $\Psi$ | $U_{tip}$ | | $\chi_{GR,YZ}$ | $\chi_{GR,XZ}$ | $\Theta_{SP}$ | $\Phi_{SP}$ | $\beta$ | $\Psi$ | $U_{tip}$ | Lag |
|---|---|---|---|---|---|---|---|---|---|---|---|---|---|---|---|---|
| –1 | 0.29 | 0.18 | 0.01 | 0.20 | 0.17 | 0.14 | 0.15 | | 0.24 | 0.10 | 0.01 | 0.20 | 0.03 | 0.20 | 0.11 | –1 |
| –½ | 0.20 | 0.27 | 0.03 | 0.08 | 0.21 | 0.22 | 0.04 | | 0.19 | 0.22 | 0.03 | 0.19 | 0.04 | 0.12 | 0.02 | –½ |
| 0 | 0.07 | 0.11 | 0 | 0.04 | 0.17 | 0.26 | 0.09 | $\bar{\theta}_{GR}$ | 0.16 | 0.10 | 0 | 0.11 | 0 | 0.24 | 0.09 | 0 |
| ½ | 0.04 | 0.14 | 0.11 | 0.04 | 0.01 | 0.23 | 0.20 | | 0.04 | 0.12 | 0.06 | 0.16 | 0.01 | 0.15 | 0.18 | ½ |
| 1 | 0.04 | 0.10 | 0.01 | 0.14 | 0.19 | 0.18 | 0.10 | | 0.17 | 0.17 | 0.01 | 0.24 | 0.06 | 0.22 | 0.09 | 1 |
| –1 | | 0.13 | 0.29 | 0.19 | 0.29 | 0.08 | 0.18 | | | 0.13 | 0.18 | 0.08 | 0.25 | 0.08 | 0.11 | –1 |
| –½ | | 0.17 | 0.25 | 0.21 | 0.24 | 0.16 | 0.25 | | | 0.17 | 0.19 | 0.10 | 0.14 | 0.16 | 0.27 | –½ |
| 0 | | 0.09 | 0.05 | 0.15 | 0.16 | 0.08 | 0.18 | $\chi_{GR,YZ}$ | | 0.09 | 0.10 | 0.12 | 0.11 | 0.08 | 0.17 | 0 |
| ½ | | 0.04 | 0.04 | 0.09 | 0.07 | 0.14 | 0.22 | | | 0.04 | 0.02 | 0.16 | 0.13 | 0.14 | 0.06 | ½ |
| 1 | | 0.07 | 0.05 | 0.08 | 0.10 | 0.15 | 0.19 | | | 0.07 | 0.05 | 0.06 | 0.19 | 0.15 | 0.11 | 1 |
| –1 | | | 0.13 | 0.12 | 0.27 | 0.15 | 0.16 | | | | 0.08 | 0.09 | 0.15 | 0.15 | 0.12 | –1 |
| –½ | | | 0.14 | 0.14 | 0.07 | 0.10 | 0.25 | | | | 0.07 | 0.16 | 0.04 | 0.10 | 0.17 | –½ |
| 0 | | | 0.19 | 0.09 | 0.11 | 0.18 | 0.12 | $\chi_{GR,XZ}$ | | | 0.14 | 0.22 | 0.14 | 0.18 | 0.11 | 0 |
| ½ | | | 0.13 | 0.18 | 0 | 0.12 | 0.28 | | | | 0.06 | 0.15 | 0.02 | 0.12 | 0.13 | ½ |
| 1 | | | 0.08 | 0.21 | 0.10 | 0.21 | 0.11 | | | | 0.14 | 0.22 | 0.07 | 0.21 | 0.10 | 1 |
| –1 | | | | 0.16 | 0.15 | 0.23 | 0.11 | | | | | 0.20 | 0.01 | 0.20 | 0.01 | –1 |
| –½ | | | | 0.13 | 0.20 | 0.18 | 0.04 | | | | | 0.08 | 0.08 | 0.18 | 0.01 | –½ |
| 0 | | | | 0.17 | 0.10 | 0.09 | 0.04 | $\Theta_{SP}$ | | | | 0.09 | 0.01 | 0.22 | 0.02 | 0 |
| ½ | | | | 0.11 | 0.13 | 0.25 | 0.14 | | | | | 0.18 | 0.04 | 0.17 | 0.03 | ½ |
| 1 | | | | 0.26 | 0.19 | 0.15 | 0.07 | | | | | 0.20 | 0.01 | 0.18 | 0.08 | 1 |
| –1 | | | | | 0.23 | 0.21 | 0.17 | | | | | | 0.17 | 0.26 | 0.20 | –1 |
| –½ | | | | | 0.22 | 0.12 | 0.19 | | | | | | 0.19 | 0.12 | 0.11 | –½ |
| 0 | | | | | 0.11 | 0.17 | 0 | $\Phi_{SP}$ | | | | | 0.11 | 0.08 | 0 | 0 |
| ½ | | | | | 0.15 | 0.15 | 0.03 | | | | | | 0.20 | 0.26 | 0.08 | ½ |
| 1 | | | | | 0.07 | 0.14 | 0.26 | | | | | | 0.20 | 0.17 | 0.19 | 1 |
| –1 | | | | | | 0.19 | 0.11 | | | | | | | 0.20 | 0.07 | –1 |
| –½ | | | | | | 0.13 | 0.07 | | | | | | | 0.17 | 0.08 | –½ |
| 0 | | | | | | 0.14 | 0.04 | $\beta$ | | | | | | 0.19 | 0.01 | 0 |
| ½ | | | | | | 0.19 | 0.12 | | | | | | | 0.24 | 0.10 | ½ |
| 1 | | | | | | 0.21 | 0.07 | | | | | | | 0.23 | 0.02 | 1 |
| –1 | | | | | | | 0.17 | | | | | | | | 0.21 | –1 |
| –½ | | | | | | | 0.11 | | | | | | | | 0.24 | –½ |
| 0 | | | | | | | 0.24 | $\Psi$ | | | | | | | 0.11 | 0 |
| ½ | | | | | | | 0.23 | | | | | | | | 0.28 | ½ |
| 1 | | | | | | | 0.33 | | | | | | | | 0.32 | 1 |

Fig. 7. Matrix of significance for cross-correlations between kinematic variables as determined by generation of the null distribution for each variable for each set of lags. The lags are defined as wingbeats with strokes representing steps of ½. The color map for probabilities ranges from red (significant for $P<0.05$) to blue (non-significant). Cross-correlations among kinematic variables on the left and right sides of the animals are provided in the left and right columns, respectively. Symbols are defined in Table 1.

mechanisms that hummingbirds use to control aerodynamic power (Chai and Dudley, 1995; Altshuler et al., 2010; Tobalske et al., 2007; Tobalske et al., 2010).

Asymmetries in the deviation path of the wings lead to the outer wing being in a more elevated position and with a higher absolute deviation in the U-shaped trajectory during both strokes as well as an increase in the stroke plane angle during the upstroke. These overall changes are apparent by comparing the time course of wing angle values in the gravitational frame of reference (Fig. 8) and by plotting the wing tip traces relative to body models in the three planes of the gravitational frame of reference (Fig. 9). Hummingbirds exhibit these stroke-specific changes in wingbeat kinematics while holding similar average body positions during stationary hovering and yaw turns to the left and right. Hummingbird yaw kinematics share similarities with measurements of attempted turns in tethered insects and real turns in freely flying insects, but also differ in key elements. Comparing hummingbird yaw turns with *Drosophila* free flight saccades (Fry et al., 2003) reveals that both animals expand the stroke amplitude of the outer wing, but the fruit flies reduce its deviation and stroke plane angle whereas the hummingbirds increase elevation amplitude ($\Theta_{SP}$) during both strokes, and stroke plane angle ($\beta$) during the upstroke. The hummingbird yaw turns also share asymmetry in inner and outer stroke amplitudes with the *Drosophila* 'sashay maneuvers' (Ristroph et al., 2009), which have a strong yaw component, but again differ with respect to deviation and stroke plane angle between the inner and outer wings.

A key turning-related kinematic feature identified from insect studies is the orientation or pitch angle of the wing in a body- or stroke-centered frame of reference, and the related angle of attack in a velocity frame of reference. Differences between inner and outer wings in the absolute rotation angles as well as the timing of rotation have been reported for tethered insects during attempted turns with varying degrees of freedom (Baker, 1979; Zarnack, 1988; Waldmann and Zarnack, 1988; Schwenne and Zarnack, 1987; Thüring, 1986; Dawson et al., 1997) and for the free flight turns of *Drosophila* (Fry et al., 2003; Ristroph et al., 2009). Our analysis did not include this feature, but there are at least two ways in which it can be very important to generating force asymmetries. Advances in the timing of wing rotation can contribute to enhanced lift (Dickinson et al., 1999), as has been demonstrated for hovering honey bees (Altshuler et al., 2005). However, even if rotational lift does not apply, left–right

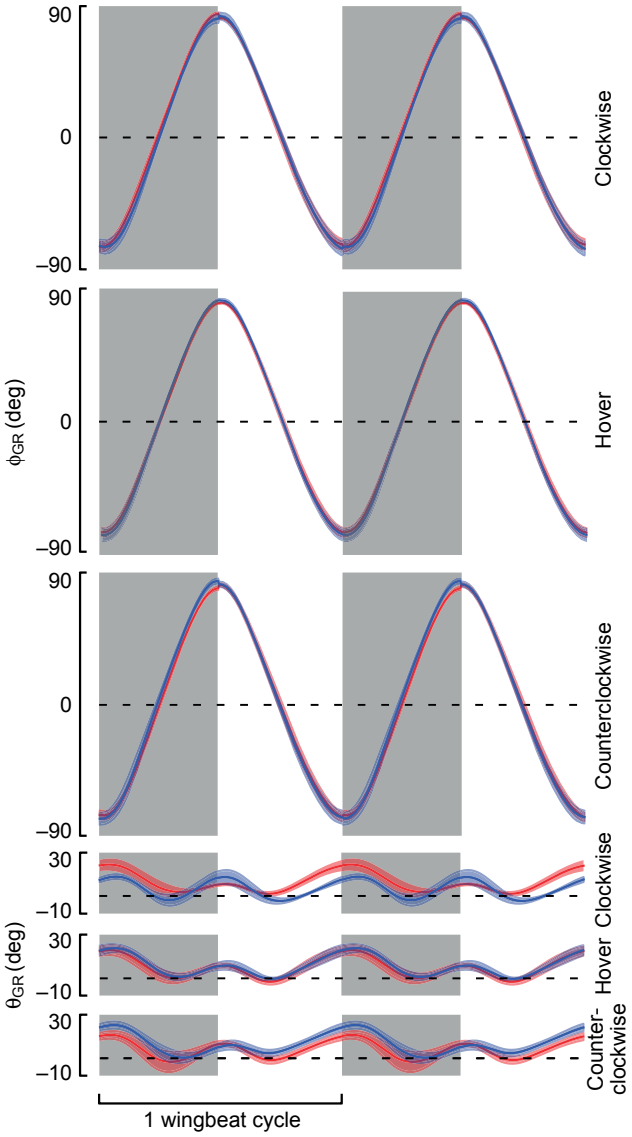


Fig. 8. Average kinematic traces in the gravitational frame of reference. The mean time course of the position angles $\phi_{GR}$ and elevation angles $\theta_{GR}$ are presented twice to allow for comparison across wingbeats. The left wing is indicated in red and the right wing is indicated in blue. Shading corresponds to the standard deviations across all four birds. Downstrokes are shaded in gray and upstrokes are in white. Discontinuities between strokes result from shifts in the frame of reference.

differences in rotation timing will influence the aerodynamic forces produced during the wing translation.

Other than hummingbirds, the birds that have been studied use fundamentally different biomechanical mechanisms to change their heading during flight. Ros et al. (Ros et al., 2011) recently demonstrated that turning in flying pigeons is controlled not by altering wingbeat kinematics but by reorienting the body to direct aerodynamic forces. They also pointed out that other birds (Warrick and Dial, 1998; Hedrick and Biewener, 2007) and bats (Aldridge, 1986; Aldridge, 1987; Iriarte-Díaz and Swartz, 2008) roll during aerial turns, which suggests that many volant vertebrates may be limited in their ability to orient aerodynamic forces off the body axis. Our results are not directly comparable with all features of the Ros et al. (Ros et al., 2011) study because we used stroke-averaged kinematics for comparisons, but the differences in stroke amplitude and deviation combined with the lack of difference in mean body position angles among flight modes indicate that hummingbirds are able to redirect forces relative to their bodies. Although Anna's hummingbirds are much smaller than the turning birds and bats that have been studied so far, there is considerable overlap in size between the larger hummingbird species and the smaller bird and bat species. Measurements from these animals would elucidate whether the differences observed so far derive from body size or from differences in body plan between hovering and non-hovering animals.

### Muscle activations

The activation bursts of the hummingbird pectoral muscles, the PM and SC, contain fewer spikes and are more advanced in relative wingbeat timing compared with the pigeon and other avian taxa (Tobalske et al., 2010). The activations of avian wing muscles have received relatively little attention with the exception of some extensive recordings with pigeons and starlings (Dial et al., 1991; Dial, 1992a; Dial, 1992b). Comparing the PS between the hummingbird and the pigeon (Dial, 1992a) reveals that the relative duration is similar between the two taxa but that the relative timing is advanced in the hummingbird. To the best of our knowledge no comparable recordings are available for the PP or FDS from other birds during flight, and it remains to be tested whether advanced timing is a feature of all hummingbird wing muscles.

The timing of muscle activations of the PM, PP and PS was more repeatable than the intensity of the activations during hovering and yaw turns (Table 4). There were no activation features consistently associated with experimental treatments, and none of the activation features were cross-correlated with kinematic variables across time. The activation timing of the PM and its antagonist, the supracoracoideus, sets the wingbeat frequency. The kinematic correlates of the activation timings of the PP and PS have not yet been described, but these may be constrained by the need to rotate the wing during stroke transition. The spike amplitude of the PM has also been demonstrated to vary consistently with the stroke amplitude as hummingbirds adjust to low air density, lift weights (Altshuler et al., 2010) or fly at faster speeds in a wind tunnel (Tobalske et al., 2010). The role of variation in the spike amplitude of the PM as well as the intensity of the PP and PS during yaw turns is not clear at the present time. It may be that wing control is best understood in terms of synergies among a larger group of muscles (d'Avella and Tresch, 2001; d'Avella et al., 2003), which has also been suggested to explain a lack of strong associations between individual muscle activation patterns and wingbeat kinematics in maneuvering cockatiels (Hedrick and Biewener, 2007).

### Time series analysis

Taking mean values of the kinematic and EMG variables and comparing these across treatments revealed significant differences in the former but not the latter. However, focusing on average values can be misleading because the animals exhibited considerable stroke-to-stroke differences, even during hovering flight. The yaw angle values did not trend monotonically during clockwise and counterclockwise feeder tracking, meaning for example that during a clockwise turn, or either of the other two treatments, the hummingbird might be yawing left, right, or holding steady during any one particular wing stroke (Fig. 1). Two distinct patterns of autocorrelation were observed, sinusoidal fluctuations and oscillations between subsequent downstrokes and upstrokes. Further analysis of the sinusoidal patterns is limited due to sample size.

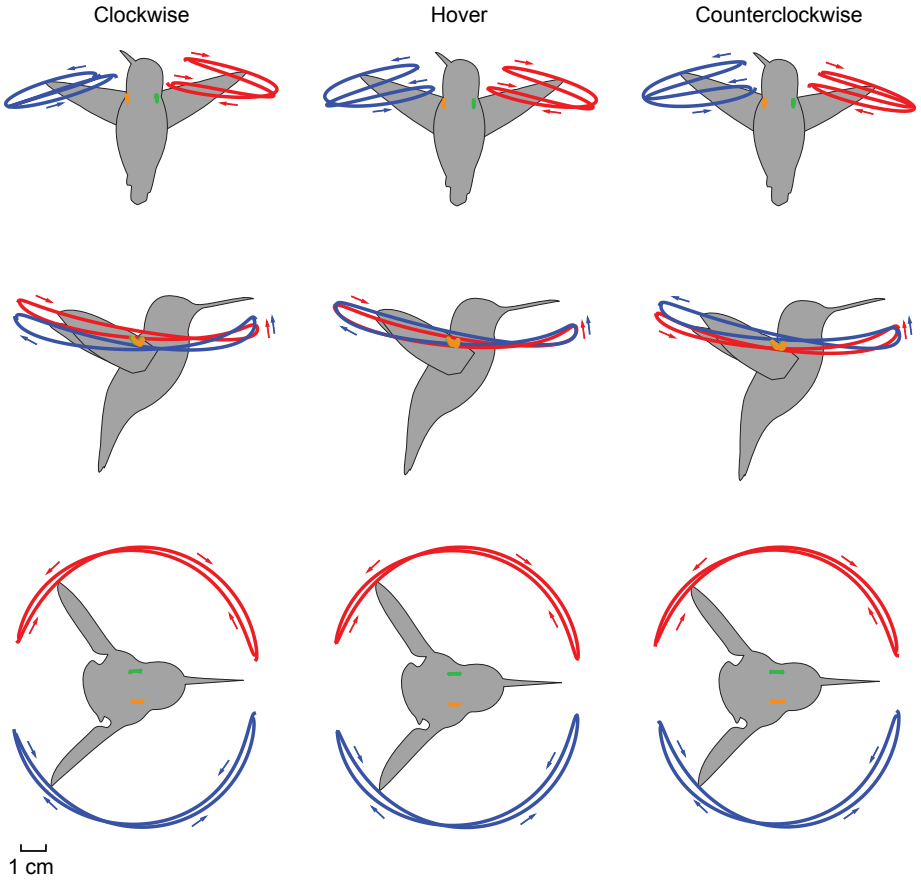


Fig. 9. Average kinematic traces plotted on the body from the front (top row), side (middle row) and top (bottom row) perspectives. Clockwise turns are depicted in the left column, hovering flight is depicted in the middle column, and counter-clockwise turns are depicted in the right column. The left wing is indicated in red and the right wing is indicated in blue. The mean values for each bird were calculated for all wingbeats in each treatment. The mean values plotted here were calculated across all four birds. Discontinuities between strokes result from shifts in the frame of reference.

Sixteen wingbeats strikes a balance between digitizing effort for a number of birds/trials and the likelihood of finding a significant temporally distant pattern. It would be highly informative to conduct a spectral analysis of wingbeat-to-wingbeat variation when more automated digitizing techniques and longer time series become available. This will also reveal whether the apparent dextral bias in some birds (Fig. 10) is an innate property or an artifact of low sample size.

Many of the kinematic features varied through time in a coordinated fashion (Fig. 7). The two strongest associations included some of the kinematic features that are also most strongly associated with feeder tracking. Wing stroke amplitude and wingtip speed were cross-correlated, indicating the importance of velocity asymmetries because the aerodynamic forces are proportional to the square of the wing velocity. The wing elevation and the elevation amplitude were also cross-correlated, indicating the importance of orientating the net force in the desired direction of movement.

We are not aware of other comparable data sets that include EMG timing and intensity measures and wingbeat kinematics on freely flying animals during sustained turns. The published measurements of wingbeat kinematics from insects and birds span several wingbeats over which the maneuver is continuously changing. In the present study, hummingbirds sustained maneuvering behavior over many wingbeats, although stroke-to-stroke variation was readily apparent. Variability of both kinematics and muscle activations has received considerable attention in the human biomechanics literature (reviewed in Stergiou and Decker, 2011). A key idea is that variation in motor features can indicate flexibility and control of complex motor behavior. For example, as humans repetitively practice some types of novel task, limb kinematics become less variable whereas EMG recordings, in contrast, can become more variable (Darling and Cooke, 1987). When increasing the speed of certain types of limb movements, the variability of both kinematics and EMG features tends to decrease (Carlton et al., 1985; Li et al., 2005). If similar principles apply to avian flight control, then the variation in muscle intensity features may be exerting a stronger influence compared with muscle timing features on stroke-to-stroke variation in wingbeat kinematics.

### Comparisons with free-flight yaw turns

The purpose of the present study was to examine the neuromuscular and kinematic mechanisms that hummingbirds employ to sustain yaw turns. The experimental approach constrained the hummingbirds to track a revolving feeder without any requirement for changes in pitch, roll, or vertical or lateral body position. As has been demonstrated for free-flying insects during turns, hummingbirds execute yaw through expansion of the outer stroke amplitude and shifts in the stroke plane and deviation path of both wings. However, we observed considerable wingbeat-to-wingbeat variation in kinematic and EMG variables, and we did not detect any consistent relationship between kinematics and muscle activations. Taken together, these results suggest that hummingbirds make fine adjustments over very short time scales to track a feeder at the angular velocities under consideration here.

To place this experimentally induced behavior in the context of more natural flight behaviors, we finally consider the distribution of yaw velocities recorded from four different *C. anna* males during solitary, feeding and competitive flights in a large flight chamber ($1.5\times1.5\times3.0$ m). The position and orientation of these birds was tracked using the Flydra system originally developed for fruit flies (Straw et al., 2011). The cameras recorded at 200 frames $s^{-1}$ and the data set comes from 44 h of recordings. The most significant

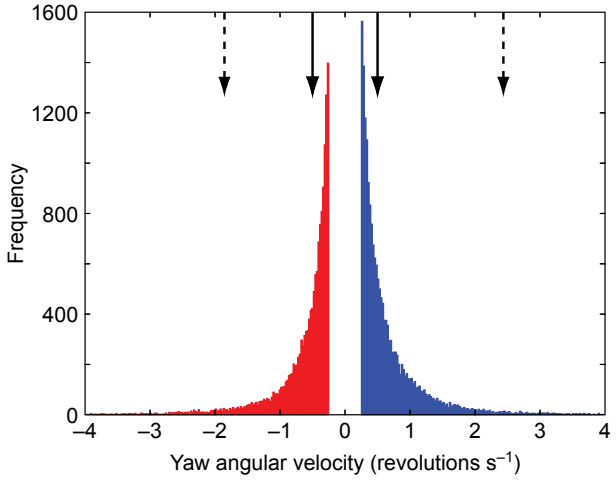


Fig. 10. Distribution of instantaneous yaw velocities recorded from the solitary and paired flights of four male *C. anna*. Values come from free-flight recordings of birds during feeding, exploratory and competitive flights. The data elements are yaw velocities >0.25 revolutions s$^{-1}$ measured from sequential frame pairs filmed at 200 frames s$^{-1}$ in which the birds held a body attitude between 60 and 80 deg relative to the horizontal plane and did not exhibit a substantial change in pitch, horizontal velocity or vertical velocity. Negative *x*-axis values indicate leftward yaw velocities (red) and positive values indicate rightward yaw velocities (blue). The solid black arrows indicate the angular velocity of the motors used for the feeder tracking experiments and the dashed black arrows represent the maximum left and right yaw velocities recorded during these experiments. The feeder tracking data are not represented in the frequency distribution of the instantaneous yaw velocities.

distinction between the free-flight yaw velocities presented in Fig. 10 and the yaw velocities from the feeder tracking experiment is that the former are determined by position differences over 5 ms whereas the latter are stroke averages over a slightly longer period of ~13 ms.

Hummingbird yaw turns from the revolving feeder experiment closely matched how they turned in free flight. The feeder was revolved by the motor at 0.5 revolutions s$^{-1}$ because this was the angular velocity at which all four birds sustained feeder tracking. This value was similar to the median free-flight yaw velocities of 0.46 and 0.48 revolutions s$^{-1}$ for the left and right turns, respectively. The maximum yaw velocities recorded during feeding tracking and free flight were also similar. The strokes with fastest yaw velocities during feeder tracking were 1.85 and 2.43 revolutions s$^{-1}$ for left and right turns, respectively. The maximum values for free-flight yaw velocities are represented by the 97.5% value of the frequency distribution, which was 2.32 and 2.33 revolutions s$^{-1}$ for left and right turns, respectively. The close correspondence in velocities indicates that the feeder tracking experiment provided a relevant test of average yaw turns. Nonetheless, it is readily apparent that tracking the revolving feeder at the imposed angular velocities required much lower values in yaw velocity than the hummingbirds are capable of performing in free flight. We conclude by suggesting that the kinematic and muscle activation variability observed during feeder tracking reflects fine motor control adjustments across wingbeats, indicating that the hummingbirds were controlling sub-maximal behavior.

## ACKNOWLEDGEMENTS

We gratefully acknowledge support from undergraduate research assistants and our colleagues. Bobby Chi, Anita Lakhani, Aleck von Mueller and Cristina Soto assisted with digitization of wingbeat kinematics. Robert Donovan, Benny Goller, Carlo Segre and Ken Welch provided technical advice. Two anonymous reviewers gave very helpful comments on the manuscript.

## FUNDING

The US National Science Foundation (IOS 0923849 and IOS 0923802) and the Natural Sciences and Engineering Research Council of Canada (402667) provided financial support during data collection, analysis and manuscript composition.

## REFERENCES

**Aldridge, H. D.** (1986). Kinematics and aerodynamics of the greater horseshoe bat, *Rhinolophus ferrumequinum*, in horizontal flight at various flight speeds. *J. Exp. Biol.* **126**, 479-497.
**Aldridge, H. D.** (1987). Turning flight of bats. *J. Exp. Biol.* **128**, 419-425.
**Altshuler, D. L., Dickson, W. B., Vance, J. T., Roberts, S. P. and Dickinson, M. H.** (2005). Short-amplitude high-frequency wing strokes determine the aerodynamics of honeybee flight. *Proc. Natl. Acad. Sci. USA* **102**, 18213-18218.
**Altshuler, D. L., Princevac, M., Pan, H. and Lozano, J.** (2009). Wake patterns of the wings and tail of hovering hummingbirds. *Exp. Fluids* **46**, 835-846.
**Altshuler, D. L., Welch, K. C., Jr, Cho, B. H., Welch, D. B., Lin, A. F., Dickson, W. B. and Dickinson, M. H.** (2010). Neuromuscular control of wingbeat kinematics in Anna's hummingbirds (*Calypte anna*). *J. Exp. Biol.* **213**, 2507-2514.
**Ando, N., Shimoyama, I. and Kanzaki, R.** (2002). A dual-channel FM transmitter for acquisition of flight muscle activities from the freely flying hawkmoth, *Agrius convolvuli*. *J. Neurosci. Methods* **115**, 181-187.
**Baker, P. S.** (1979). The wing movements of flying locusts during steering behaviour. *J. Comp. Physiol. A* **131**, 49-58.
**Balint, C. N. and Dickinson, M. H.** (2001). The correlation between wing kinematics and steering muscle activity in the blowfly *Calliphora vicina*. *J. Exp. Biol.* **204**, 4213-4226.
**Carlton, M. J., Robertson, R. N., Carlton, L. G. and Newell, K. M.** (1985). Response timing variability: coherence of kinematic and EMG parameters. *J. Mot. Behav.* **17**, 301-319.
**Carrier, D. R., Walter, R. M. and Lee, D. V.** (2001). Influence of rotational inertia on turning performance of theropod dinosaurs: clues from humans with increased rotational inertia. *J. Exp. Biol.* **204**, 3917-3926.
**Chai, P. and Dudley, R.** (1995). Limits to vertebrate locomotor energetics suggested by hummingbirds hovering in heliox. *Nature* **377**, 722-725.
**Clark, C. J.** (2011). Effects of tail length on an escape maneuver of the red-billed streamertail. *J. Ornithol.* **152**, 397-408.
**Cowpertwait, P. S. P. and Metcalfe, A. V.** (2009). *Introductory Time Series with R*. New York: Springer.
**d'Avella, A. and Tresch, M. C.** (2001). Modularity in the motor system: decomposition of muscle patterns as combinations of time-varying synergies. In *Advances in Neural Information Processing Systems 14* (ed. T. G. Dietterich, S. Becker and Z. Ghahramani), pp. 141-148. Cambridge, MA: MIT Press.
**d'Avella, A., Saltiel, P. and Bizzi, E.** (2003). Combinations of muscle synergies in the construction of a natural motor behavior. *Nat. Neurosci.* **6**, 300-308.
**Darling, W. G. and Cooke, W. G.** (1987). Movement related EMGs become more variable during learning of fast accurate movements. *J. Mot. Behav.* **19**, 311-331.
**Dawson, J., Dawson-Scully, K., Robert, D. and Robertson, R. M.** (1997). Forewing asymmetries during auditory avoidance in flying locusts. *J. Exp. Biol.* **200**, 2323-2335.
**Dial, K. P.** (1992a). Activity patterns of the wing muscles of the pigeon (*Columba livia*) during different modes of flight. *J. Exp. Zool.* **262**, 357-373.
**Dial, K. P.** (1992b). Avian forelimb muscles and nonsteady flight: can birds fly without using the muscles in their wings? *Auk* **109**, 874-885.
**Dial, K. P., Goslow, G. E. and Jenkins, F. A., Jr** (1991). The functional anatomy of the shoulder in the European starling (*Sturnus vulgaris*). *J. Morphol.* **207**, 327-344.
**Dickinson, M. H., Lehmann, F.-O. and Sane, S. P.** (1999). Wing rotation and the aerodynamic basis of insect flight. *Science* **284**, 1954-1960.
**Dudley, R.** (2000). *The Biomechanics of Insect Flight*. Princeton, NJ: Princeton University Press.
**Eilam, D.** (1994). Influence of body morphology on turning behavior in carnivores. *J. Mot. Behav.* **26**, 3-12.
**Ellington, C. P.** (1984). The aerodynamics of hovering insect flight. II. Morphological parameters. *Philos. Trans. R. Soc. Lond.* B **305**, 17-40.
**Fry, S. N., Sayaman, R. and Dickinson, M. H.** (2003). The aerodynamics of free-flight maneuvers in *Drosophila*. *Science* **300**, 495-498.
**Götz, K. G.** (1968). Flight control in *Drosophila* by visual perception of motion. *Kybernetik* **4**, 199-208.
**Hagiwara, S., Chichibu, S. and Simpson, N.** (1968). Neuromuscular mechanisms of wing beat in hummingbirds. *Z. Vgl. Physiol.* **60**, 209-218.
**Hedenström, A. and Rosén, M.** (2001). Predator versus prey: on aerial hunting and escape strategies in birds. *Behav. Ecol.* **12**, 150-156.
**Hedrick, T. L.** (2008). Software techniques for two- and three-dimensional kinematic measurements of biological and biomimetic systems. *Bioinspir. Biomim.* **3**, 034001.
**Hedrick, T. L. and Biewener, A. A.** (2007). Low speed maneuvering flight of the rose-breasted cockatoo (*Eolophus roseicapillus*). I. Kinematic and neuromuscular control of turning. *J. Exp. Biol.* **210**, 1897-1911.
**Hedrick, T. L., Usherwood, J. R. and Biewener, A. A.** (2007). Low speed maneuvering flight of the rose-breasted cockatoo (*Eolophus roseicapillus*). II. Inertial and aerodynamic reorientation. *J. Exp. Biol.* **210**, 1912-1924.
**Hedrick, T. L., Cheng, B. and Deng, X.** (2009). Wingbeat time and the scaling of passive rotational damping in flapping flight. *Science* **324**, 252-255.
**Heide, G.** (1975). Properties of a motor output system involved in the optomotor response in flies. *Biol. Cybern.* **20**, 99-112.

**Hothorn, T., Bretz, F. and Westfall, P.** (2008). Simultaneous inference in general parametric models. *Biom. J.* **50**, 346-363.
**Iriarte-Díaz, J. and Swartz, S. M.** (2008). Kinematics of slow turn maneuvering in the fruit bat *Cynopterus brachyotis*. *J. Exp. Biol.* **211**, 3478-3489.
**Lee, D. V., Walter, R. M., Deban, S. M. and Carrier, D. R.** (2001). Influence of increased rotational inertia on the turning performance of humans. *J. Exp. Biol.* **204**, 3927-3934.
**Lehmann, F.-O. and Götz, K. G.** (1996). Activation phase ensures kinematic efficacy in flight-steering muscles of *Drosophila melanogaster*. *J. Comp. Physiol. A* **179**, 311-322.
**Lessells, C. M. and Boag, P. T.** (1987). Unrepeatable repeatabilities: a common mistake. *Auk* **104**, 116-121.
**Li, L., Haddad, J. M. and Hamill, J.** (2005). Stability and variability may respond differently to changes in walking speed. *Hum. Mov. Sci.* **24**, 257-267.
**Nakagawa, S. and Schielzeth, H.** (2010). Repeatability for Gaussian and non-Gaussian data: a practical guide for biologists. *Biol. Rev. Camb. Philos. Soc.* **85**, 935-956.
**Norberg, U. M. and Rayner, J. M. V.** (1987). Ecological morphology and flight in bats (Mammalia; Chiroptera): wing adaptations, flight performance, foraging strategy and echolocation. *Philos. Trans. R. Soc. Lond. B* **316**, 335-427.
**Pennycuick, C. J.** (1975). Mechanics of flight. In *Avian Biology* (ed. D. S. Farner, J. R. King and K. C. Parkes), pp. 1-75. London: Academic Press.
**R Development Core Team** (2012). R: A Language and Environment for Statistical Computing. Version 2.15.0. Vienna, Austria: R Foundation for Statistical Computing.
**Ristroph, L., Berman, G. J., Bergou, A. J., Wang, Z. J. and Cohen, I.** (2009). Automated hull reconstruction motion tracking (HRMT) applied to sideways maneuvers of free-flying insects. *J. Exp. Biol.* **212**, 1324-1335.
**Ros, I. G., Bassman, L. C., Badger, M. A., Pierson, A. N. and Biewener, A. A.** (2011). Pigeons steer like helicopters and generate down- and upstroke lift during low speed turns. *Proc. Natl. Acad. Sci. USA* **108**, 19990-19995.
**Russell, S. M. and Russell, R. O.** (2001). *The North American Banders' Manual for Banding Hummingbirds*. Point Reyes Station, CA: The North American Banding Council.
**Schwenne, T. and Zarnack, W.** (1987). Movements of the hindwings of *Locusta migratoria*, measured with miniature coils. *J. Comp. Physiol. A* **160**, 657-666.
**Springthorpe, D., Fernández, M. J. and Hedrick, T. L.** (2012). Neuromuscular control of free-flight yaw turns in the hawkmoth *Manduca sexta*. *J. Exp. Biol.* **215**, 1766-1774.
**Stergiou, N. and Decker, L. M.** (2011). Human movement variability, nonlinear dynamics, and pathology: is there a connection? *Hum. Mov. Sci.* **30**, 869-888.
**Straw, A. D., Branson, K., Neumann, T. R. and Dickinson, M. H.** (2011). Multi-camera real-time three-dimensional tracking of multiple flying animals. *J. R. Soc. Interface* **8**, 395-409.
**Thüring, D. A.** (1986). Variability of motor output during flight steering in locusts. *J. Comp. Physiol. A* **158**, 653-664.
**Tobalske, B. W., Warrick, D. R., Clark, C. J., Powers, D. R., Hedrick, T. L., Hyder, G. A. and Biewener, A. A.** (2007). Three-dimensional kinematics of hummingbird flight. *J. Exp. Biol.* **210**, 2368-2382.
**Tobalske, B. W., Biewener, A. A., Warrick, D. R., Hedrick, T. L. and Powers, D. R.** (2010). Effects of flight speed upon muscle activity in hummingbirds. *J. Exp. Biol.* **213**, 2515-2523.
**Tu, M. S. and Dickinson, M. H.** (1996). The control of wing kinematics by two steering muscles of the blowfly (*Calliphora vicina*). *J. Comp. Physiol. A* **178**, 813-830.
**Venables, W. N. and Ripley, B. D.** (2002). *Modern Applied Statistics with S*, 4th edn. New York: Springer.
**Waldmann, B. and Zarnack, W.** (1988). Forewing movements and motor activity during roll manoeuvers in flying desert locusts. *Biol. Cybern.* **59**, 325-335.
**Wang, H., Ando, N. and Kanzaki, R.** (2008). Active control of free flight manoeuvres in a hawkmoth, *Agrius convolvuli*. *J. Exp. Biol.* **211**, 423-432.
**Warrick, D. R. and Dial, K. P.,** (1998). Kinematic, aerodynamic and anatomical mechanisms in the slow, maneuvering flight of pigeons. *J. Exp. Biol.* **201**, 655-672.
**Warrick, D. R., Dial, K. P. and Biewener, A. A.** (1988). Asymmetrical force production in the maneuvering flight of pigeons. *Auk* **115**, 916-928.
**Webb, P. W.** (1983). Speed, acceleration and manoeuvrability of two teleost fishes. *J. Exp. Biol.* **102**, 115-122.
**Weihs, D.** (1972). A hydrodynamical analysis of fish turning manoeuvres. *Proc. R. Soc. B* **182**, 59-72.
**Welch, K. C., Jr and Altshuler, D. L.** (2009). Fiber type homogeneity of the flight musculature in small birds. *Comp. Biochem. Physiol.* **152B**, 324-331.
**Whitlock, M. C. and Schluter, D.** (2009). *The Analysis of Biological Data*. Greenwood Village, CO: Roberts and Company Publishers.
**Zarnack, W.** (1988). The effect of forewing depressor activity on wing movement during locust flight. *Biol. Cybern.* **59**, 55-70.

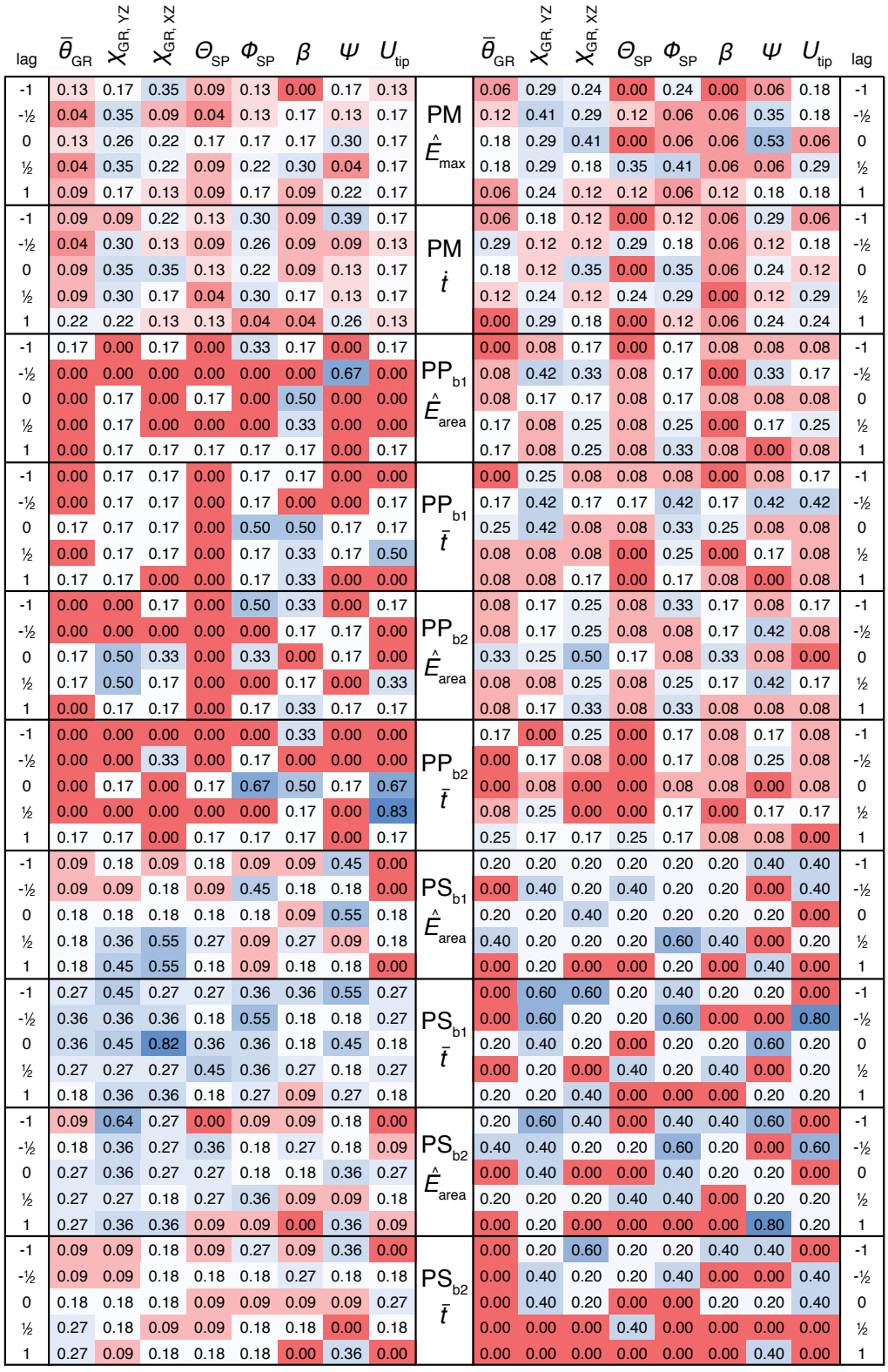


Fig. S1. Matrix showing the proportion of cross-correlations between kinematic and electromyographic variables with *P*-values <0.05 before correcting for multiple comparisons. The lags are defined as wingbeats with strokes representing steps of ½. The color map for proportions ranges from red (none of the cross-correlation pairs are significant) to blue (most of the of cross-correlation pairs are significant). The kinematic variables include the average elevation angle ($\bar{\theta}_{GR}$), body angle frontal ($\chi_{GR,YZ}$), body angle lateral ($\chi_{GR,XZ}$), elevation amplitude ($\Theta_{SP}$), stroke amplitude ($\Phi_{SP}$), stroke plane angle ($\beta$), yaw angle ($\Psi$) and wingtip speed ($U_{tip}$). Muscle variables include the occurrence of the first spike ($\dot{t}$) and the normalized maximum spike amplitude ($\hat{E}_{max}$) of the pectoralis major (PM), and the average spike occurrence ($\bar{t}$) and rectified area of the waveform ($\hat{E}_{area}$) of bursts 1 and 2 of the pronator profundus (PP) and pronator superficialis (PS). Cross-correlations among kinematic variables on the left side of the animals are provided in the left columns and cross-correlations among kinematics on the right side are shown in the right columns.

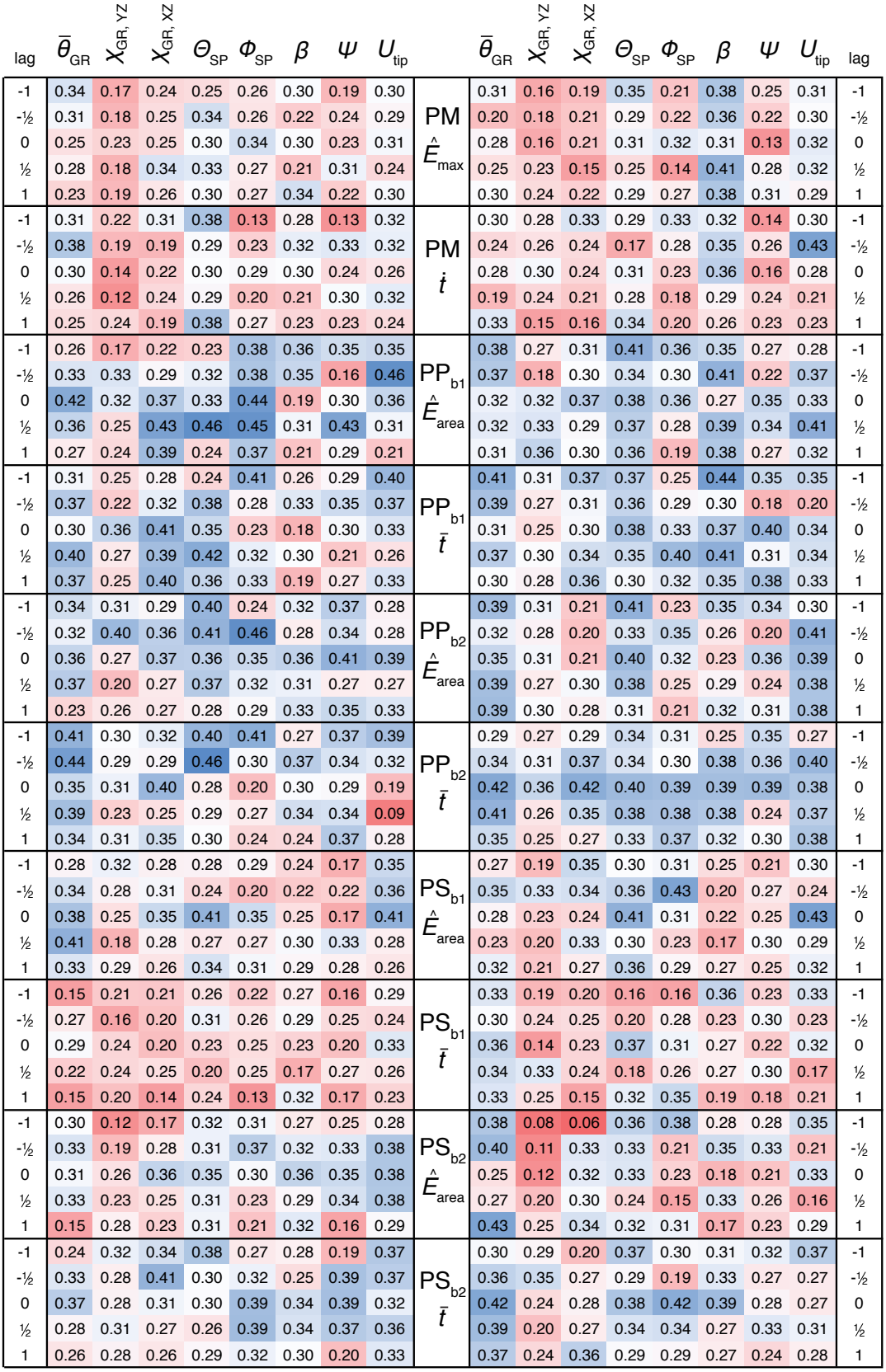


Fig. S2. Matrix of significance for cross-correlations between kinematic and electromyographic variables as determined by generation of the null distribution for each variable for each set of lags. The color map for probabilities ranges from red (strong trends but non-significant) to blue (non-significant). Symbols and arrangements for the variables are given in Table 1 and supplementary material Fig. S1.

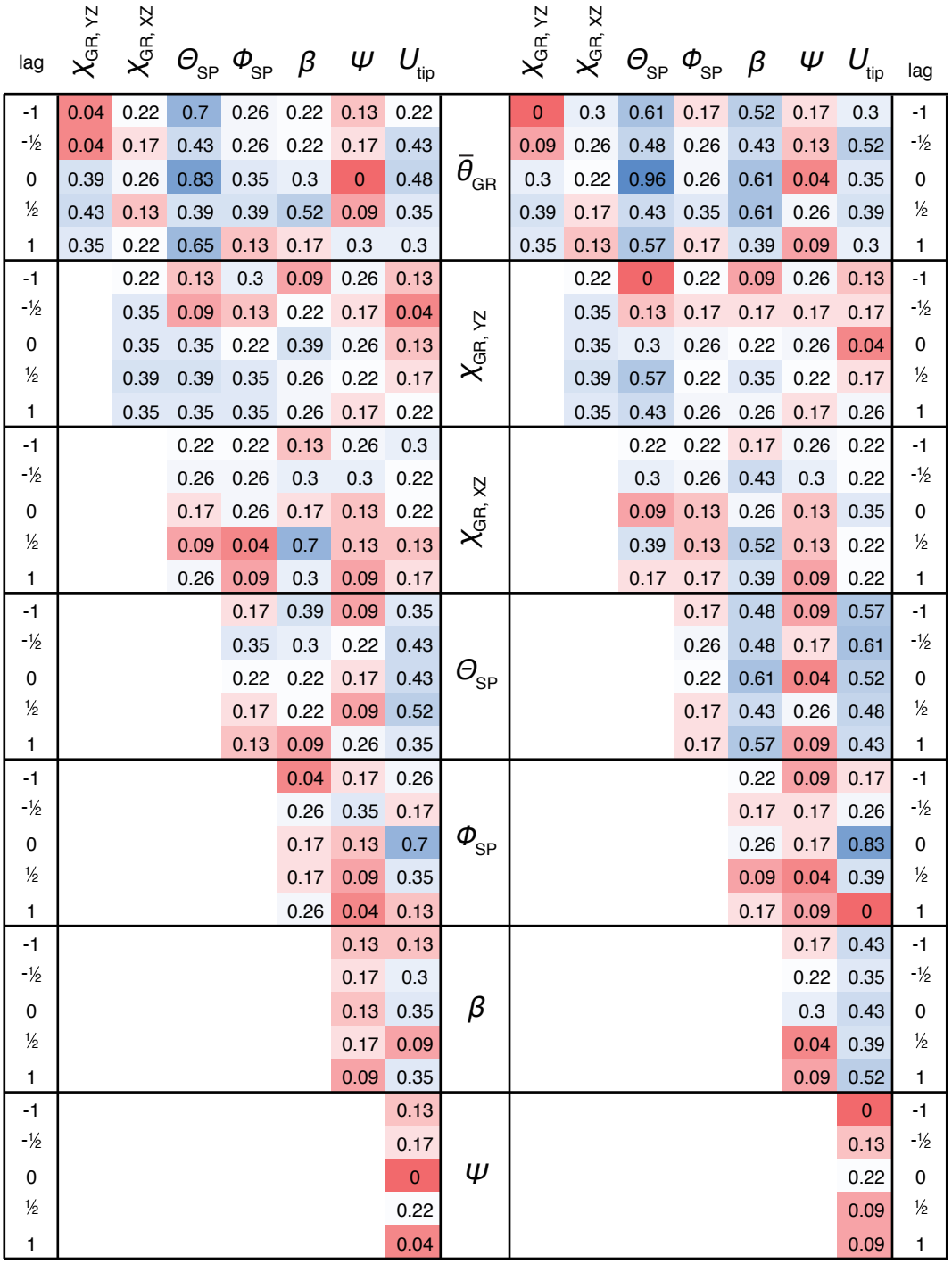


Fig. S3. Matrix showing the proportion of cross-correlations between kinematic variables with *P*-values <0.05 before correcting for multiple comparisons. The color map for proportions ranges from red (none of the cross-correlation pairs are significant) to blue (most of the of cross-correlation pairs are significant). Symbols and arrangements for the kinematic variables are given as in Table 1 and Fig. 7.

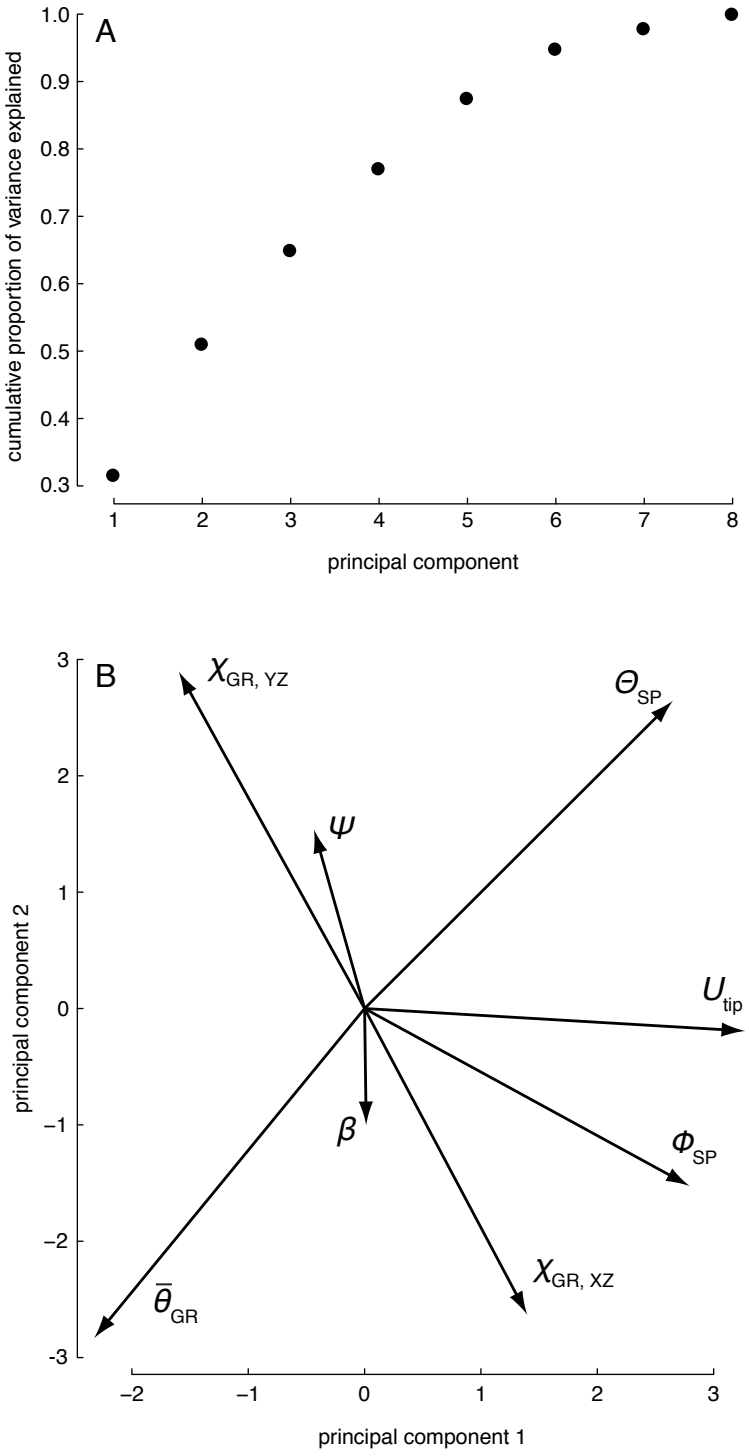


Fig. S4. Results of principal components analysis of kinematic measures. (A) Cumulative proportion of variance explained by the eight principal components. In contrast to most PCA analyses, the cumulative proportion of variance explained increases almost linearly over the first six PCs. The first two PCs only account for 51% of the variance. (B) Biplot of PC2 *versus* PC1 with arrows showing the loading vectors for each of the kinematic measures. With the exception of body angle frontal and yaw angle, no two variables load together consistently on PC1 and PC2.

Table S1. The proportions of trials with significant autocorrelation (identified as those with at least one lag correlation falling outside the 95% confidence interval) for each of the kinematic and EMG variables arranged by flight mode

| | Maneuver | | |
|---|---|---|---|
| Variable | Clockwise | Hovering | Counterclockwise |
| $\Psi$ | 0.25 | 0.43 | 0.62 |
| $U_{tip}$ | 0.62 | 0.71 | 0.81 |
| $\chi_{GR,XZ}$ | 1.00 | 1.00 | 1.00 |
| $\chi_{GR,YZ}$ | 0.88 | 1.00 | 0.75 |
| $\bar{\theta}_{GR}$ | 0.94 | 0.79 | 1.00 |
| $\beta$ | 0.94 | 0.71 | 0.81 |
| $\Phi_{SP}$ | 0.56 | 0.57 | 0.62 |
| $\Theta_{SP}$ | 0.69 | 0.86 | 0.94 |
| $t_{PM}$ | 0.21 | 0.08 | 0.36 |
| $\hat{E}_{max,PM}$ | 0.57 | 0.33 | 0.71 |
| $\tilde{t}_{PS,1}$ | 0.50 | 0.50 | 0.67 |
| $\tilde{t}_{PS,2}$ | 0.50 | 0 | 0.17 |
| $\hat{E}_{area,PS,1}$ | 0.50 | 0.50 | 0.50 |
| $\hat{E}_{area,PS,2}$ | 0.50 | 0 | 0.50 |
| $\tilde{t}_{PP,1}$ | 0.67 | 0.33 | 0.67 |
| $\tilde{t}_{PP,2}$ | 0.50 | 0.33 | 0.50 |
| $\hat{E}_{area,PP,1}$ | 0.50 | 0.50 | 0.67 |
| $\hat{E}_{area,PP,2}$ | 0.33 | 0.17 | 0 |

The analysis was performed after correcting for non-stationarity of the sequences. Symbols as in Table 1.

Table S2. Results of principal components analysis among nine kinematic measures

| | PC1 | PC2 | PC3 | PC4 | PC5 | PC6 | PC7 | PC8 |
|---|---|---|---|---|---|---|---|---|
| Variance | 0.32 | 0.19 | 0.14 | 0.12 | 0.10 | 0.07 | 0.03 | 0.02 |
| Cumulative variance | 0.32 | 0.51 | 0.65 | 0.77 | 0.87 | 0.95 | 0.98 | 1.00 |
| Loadings | | | | | | | | |
| $\Psi$ | –0.07 | 0.24 | 0.47 | 0.63 | –0.56 | 0.01 | –0.02 | 0.02 |
| $U_{tip}$ | 0.55 | –0.03 | –0.13 | 0.33 | 0.15 | 0.05 | –0.03 | –0.74 |
| $\chi_{GR,XZ}$ | 0.23 | –0.44 | 0.37 | –0.31 | –0.26 | 0.67 | 0.09 | –0.03 |
| $\chi_{GR,YZ}$ | –0.27 | 0.48 | –0.22 | 0.19 | 0.28 | 0.71 | 0.18 | 0 |
| $\bar{\theta}_{GR}$ | –0.39 | –0.48 | –0.06 | 0.32 | 0.18 | 0.17 | –0.67 | –0.03 |
| $\beta$ | 0 | –0.15 | –0.75 | 0.06 | –0.63 | 0.09 | 0.05 | 0.04 |
| $\Phi_{SP}$ | 0.47 | –0.25 | –0.10 | 0.45 | 0.28 | 0.04 | 0.19 | 0.63 |
| $\Theta_{SP}$ | 0.45 | 0.45 | –0.04 | –0.22 | –0.09 | 0.12 | –0.69 | 0.24 |

The first two rows give the proportion of variance explained and cumulative proportion of variance explained by the eight principal components (PCs). Principal component loadings for each of the eight kinematic measures are given for each PC. Kinematic symbols as in Table 1.